On-shell versus curvature mass parameter fixing schemes in the quark-meson model and its phase diagrams

Suraj Kumar Rai[1,2,*] and Vivek Kumar Tiwari[1,†]

[1]Department of Physics, University of Allahabad, Prayagraj, India-211002
[2]Department of Physics, A.N.D. Kisan P.G. College Babhnan Gonda, Dr. R.M.L. Awadh University, Faizabad, India-271313

(Received 24 February 2022; accepted 25 April 2022; published 16 May 2022)

We compute and compare the effective potential and phase structure for the quark-meson model in an extended mean-field approximation when vacuum one-loop quark fluctuations are included and the model parameters are fixed using different renormalization prescriptions. When the quark one-loop vacuum divergence is regularized under the minimal subtraction scheme, the fixing of the model parameters using the curvature masses of the scalar and pseudoscalar mesons has been termed as the quark-meson model with the vacuum term (QMVT). However, this prescription becomes inconsistent when we notice that the curvature mass is akin to defining the meson mass by the self-energy evaluation at vanishing momentum. In this work, we apply the recently reported exact prescription of the on-shell parameter fixing to that version of quark-meson model where the two quark flavors are coupled to the eight mesons of the $SU_L(2) \times SU_R(2)$ linear sigma model with isosinglet σ (η), isotriplet $\vec{a}_0$ ($\vec{\pi}$) scalar (pseudoscalar) mesons. The model then becomes the renormalized quark-meson (RQM) model where physical (pole) masses of mesons and pion decay constant are put into the relation of the running mass parameter and couplings by using the on-shell and the minimal subtraction renormalization schemes. The vacuum effective potential plots, the phase diagrams and the order parameter temperature variations for both the RQM model and the QMVT model are exactly identical for the $m_\sigma = 616$ MeV. The vacuum effective potential, when the $m_\sigma < 616$ MeV, is deepest for the QMVT model. An interesting trend reversal is observed for the $m_\sigma > 616$ MeV when the effective potential of the RQM model becomes deepest. We find similar m_σ dependent differences in the nature of the RQM and QMVT model phase diagrams and the order parameter temperature variations. Furthermore, $SU_A(2)$ chiral and $U_A(1)$ axial symmetry breaking/restoration and their interplay can also be investigated in this framework.

DOI: 10.1103/PhysRevD.105.094010

I. INTRODUCTION

A strong interaction theory motivated first quantum chromodynamics (QCD) schematic phase diagram appeared in the 1970s [1]. It projected a confined phase of hadrons at low temperature and baryonic density, and a deconfined phase of quarks and gluons at high temperature or baryonic density [2–5]. Mapping out the QCD phase diagram in all its details is still a very active area of current research as it is not very well understood. The first-principle lattice QCD simulations [6–14] provide us valuable information for the QCD phase transition but the real progress in the lattice QCD calculations gets seriously bogged down by the QCD action becoming complex due to the fermion sign problem [8] when baryon density/chemical potential becomes nonzero. The phenomenological models developed with the effective degrees of freedom [15,16] are of great help in mapping out the phase diagram in the regions inaccessible to the lattice simulations.

The QCD Lagrangian for the two flavor of massless quarks has the $SU_{L+R}(2) \times SU_{L-R}(2)$ symmetry. The axial (A = L − R) part of the symmetry called the chiral symmetry gets spontaneously broken in the low energy hadronic vacuum of the QCD as the chiral condensate forms and one gets three massless pions as Goldstone bosons. The chiral symmetry gets explicitly broken as well, due to the small mass of the u and d quarks and we find light pions in the nature. The $SU_L(2) \times SU_R(2)$ linear sigma model provides us a good framework [17–19] in which the chiral $SU_A(2)$ symmetry and the axial $U_A(1)$ symmetry breaking and restoration both can be investigated in great detail as it enables the construction of chiral invariant combinations using the chiral partners from the isosinglet σ and the isoriplet $\vec{a}_0$ scalar mesons to the isosinglet η and isotriplet $\vec{\pi}$

*surajrai050@gmail.com
†vivekkrt@gmail.com

pseudoscalar mesons. Coupling these eight scalar and pseudoscalar meson degrees of freedom to the two flavor of quarks, we get the QCD-like framework of the quark-meson (QM) model in which we can compute and explore the QCD phase diagram.

Furthermore, at low temperatures and densities, the confinement of quarks inside the hadrons also gets implemented by the introduction of the Polyakov loop where the QCD confinement is mimicked in a statistical sense by coupling the chiral models to a constant background $SU(N_c)$ gauge field A_μ^a [20–24]. Using phenomenological Polyakov loop potential [25,26], the free energy density from the gluons is added to the QM model and it becomes the PQM model. Several investigations of the QCD phase structure/phase diagram have already been done in the chiral models [27–38], two and three flavor QM model [39–42] and PQM model [43–46].

Under the "no-Dirac sea" or standard mean field approximation (S-MFA), fermionic vacuum fluctuations and renormalization issues are neglected altogether [27,33,39–46] assuming that the redefined meson potential parameters would reabsorb their effects. This familiar setting of the QM model gives an inconsistent result as in the chiral limit, one gets a first-order chiral phase transition at zero baryon densities which is at odds with the general theoretical arguments [47,48]. The proper treatment of the Dirac sea, first proposed in the Ref. [49], remedied the above inconsistency. Later several research papers [50–63] worked out the detailed impact of including the quark one-loop vacuum correction in the two and three flavor QM/PQM model. The minimal subtraction scheme is used to properly regularize the quark one-loop vacuum divergence in these publications. Then the model parameters are fixed by using the σ and π meson curvature mass, defined by the second derivative of the thermodynamic potential at its minimum. Furthermore, the vacuum expectation value of the sigma mean field is put equal to the pion decay constant. Since the effective potential generates the n-point functions of the theory at vanishing external momenta, the curvature mass is akin to defining the meson mass by the evaluation of self-energy at zero momentum [64–68]. This consideration renders the above parameter fixing procedure inconsistent. In order to make comparisons and quantify the effect of the parameter fixing with the curvature meson masses, we have named this model setting as the quark-meson model with vacuum term (QMVT).

The six parameters, λ_1, λ_2, t'Hooft coupling c, mass parameter m^2, explicit symmetry breaking strength h and Yukawa coupling g of the QM model Lagrangian, are determined by the physical values of the m_σ, m_π, eta meson mass m_η, isotriplet scalar meson mass $m_{\vec{a}_0}$, constituent quark mass m_q and pion decay constant f_π. It is to be noted that in most renormalization procedures, radiative corrections to the physical quantities change their tree-level relations to the parameters of the Lagrangian. Thus the use of tree-level values of the parameters in the effective potential calculation becomes inconsistent. The $\overline{\text{MS}}$ scheme running parameters depend on the renormalization scale Λ whereas the on-shell parameters have their tree-level values. The correct renormalization prescription allows us to calculate the counterterms both in the $\overline{\text{MS}}$ scheme and in the on-shell scheme and then the renormalized parameters of the two schemes get connected. The effective potential is then calculated using the modified minimal subtraction procedure where the relations between the running parameters and the on-shell parameters (physical quantities) are used as input [65]. Adhikari and collaborators in a series of papers [65,69–71] used this renormalization prescription to correctly account for the effect of Dirac sea in the context of QM model where $O(4)$ sigma model has been used for the mesonic degree of freedom (isosinglet scalar meson σ and isotriplet π). In the present work, we are applying this prescription of the on-shell parameter fixing to that version of the quark-meson (QM) model in which the two flavor of quarks are coupled to the eight mesons of the $SU_L(2) \times SU_R(2)$ linear sigma model with isosinglet σ, isotriplet $\vec{a}_0$ scalar mesons and isosinglet η, isotriplet $\vec{\pi}$ pseudoscalar mesons. We have termed this model setting as the renormalized quark-meson (RQM) model which has the advantage of providing us the framework in which, apart from the $SU_A(2)$ chiral, we can investigate the $U_A(1)$ axial symmetry breaking and restoration also together with the interplay of axial $U_A(1)$ and $SU_A(2)$ chiral symmetry.

The paper is arranged as follows. The brief formulation of the $SU_L(2) \times SU_R(2)$ QM model is presented in Sec. II. Section III presents the calculation of the effective potential of the quark-meson model with vacuum term (QMVT). The parameter fixing procedure using the curvature masses of the scalar and pseudoscalar mesons has also been explained here. The on-shell scheme counterterms and self-energy calculations are presented in Sec. IV A. The relations between the physical quantities and the running parameters are derived in Sec. IV B; the derivation of the effective potential in the RQM model is also presented in Sec. IV C. The result and discussion is presented in Sec. V. Finally, the summary and conclusion are presented in Sec. VI.

II. MODEL FORMULATION

The $SU_L(2) \times SU_R(2)$ quark-meson model formulation will be presented in this section. In the two flavor quark-meson model, two light quarks and $SU_V(2) \times SU_A(2)$ symmetric meson fields are coupled together. The Lagrangian of the model [17–19] is written as

$$\begin{aligned}\mathcal{L}_{QM} = \bar{\psi}[i\gamma^\mu\partial_\mu - gt_0(\sigma + i\gamma_5\eta) \\ - g\vec{t}\cdot(\vec{a} + i\gamma_5\vec{\pi})]\psi + \mathcal{L}(\mathcal{M}),\end{aligned} \tag{1}$$

where ψ is a color N_c-plet, a four-component Dirac spinor as well as a flavor doublet

$$\psi = \begin{pmatrix} u \\ d \end{pmatrix}. \tag{2}$$

The Lagrangian for meson fields is [17]

$$\begin{aligned}\mathcal{L}(\mathcal{M}) = {} & \mathrm{Tr}(\partial_\mu \mathcal{M}^\dagger \partial^\mu \mathcal{M} - m^2(\mathcal{M}^\dagger \mathcal{M})) \\ & - \lambda_1[\mathrm{Tr}(\mathcal{M}^\dagger \mathcal{M})]^2 - \lambda_2 \mathrm{Tr}(\mathcal{M}^\dagger \mathcal{M})^2 \\ & + c[\det \mathcal{M} + \det \mathcal{M}^\dagger] + \mathrm{Tr}[H(\mathcal{M} + \mathcal{M}^\dagger)]. \end{aligned} \tag{3}$$

Here field $\mathcal{M}$ is a complex 2×2 matrix

$$\mathcal{M} = t_a \xi_a = t_a(\sigma_a + i\pi_a),$$

$a = 0$, 1, 2, and 3. t_a represents the four generators of the $U(2)$ algebra:

$$\begin{aligned}\mathcal{M} &= t_0(\sigma_0 + i\pi_0) + \vec{t} \cdot (\vec{\sigma} + i\vec{\pi}) \\ &= t_0(\sigma + i\eta) + \vec{t} \cdot (\vec{a} + i\vec{\pi}) \end{aligned} \tag{4}$$

with $t_0 = \frac{1}{2}\left(\begin{smallmatrix} 1 & 0 \\ 0 & 1 \end{smallmatrix}\right)$, $t_1 = \frac{1}{2}\left(\begin{smallmatrix} 0 & 1 \\ 1 & 0 \end{smallmatrix}\right)$, $t_2 = \frac{1}{2}\left(\begin{smallmatrix} 0 & -i \\ i & 0 \end{smallmatrix}\right)$, and $t_3 = \frac{1}{2}\left(\begin{smallmatrix} 1 & 0 \\ 0 & -1 \end{smallmatrix}\right)$.

One can rewrite the Lagrangian (3) in the form [18]

$$\begin{aligned}\mathcal{L}(\mathcal{M}) = {} & \frac{1}{2}(\partial_\mu \sigma \partial_\mu \sigma + \partial_\mu \vec{\pi} \cdot \partial_\mu \vec{\pi} + \partial_\mu \eta \partial_\mu \eta \\ & + \partial_\mu \vec{a_0} \cdot \partial_\mu \vec{a_0}) - U. \end{aligned} \tag{5}$$

Further

$$\begin{aligned} U(\sigma, \vec{a}_0, \vec{\pi}, \eta) = {} & \frac{m^2}{2}(\sigma^2 + \vec{\pi}^2 + \eta^2 + \vec{a}_0^2) - h\sigma \\ & + \frac{1}{4}\left(\lambda_1 + \frac{1}{2}\lambda_2\right)(\sigma^2 + \vec{\pi}^2 + \eta^2 + \vec{a}_0^2)^2 \\ & + \frac{\lambda_2}{2}\{(\sigma^2 + \vec{\pi}^2)(\eta^2 + \vec{a}_0^2) \\ & - (\sigma\eta - \vec{\pi} \cdot \vec{a}_0)^2\} \\ & - \frac{c}{2}(\sigma^2 - \eta^2 + \vec{\pi}^2 - \vec{a}_0^2). \end{aligned} \tag{6}$$

The 2×2 matrix H explicitly breaks the chiral symmetry and is chosen as

$$H = t_a h_a, \tag{7}$$

where h_a are external fields. The field σ acquires nonzero vacuum expectation value (VEV) $\bar{\sigma}$, due to the spontaneous breaking of the chiral symmetry, while the other scalar and pseudoscalar fields ($\vec{a}_0$, $\vec{\pi}$, η) assume zero VEV. Here the two parameters h_0 and h_3 may give rise to the explicit breaking of chiral symmetry. We are neglecting the isospin symmetry breaking, hence we choose $h_0 \neq 0$ and $h_3 = 0$.

The field σ has to be shifted to $\sigma \to \bar{\sigma} + \sigma$ as it acquires nonzero VEV. The tree-level curvature masses of mesons as evaluated in Ref. [17] are written as

$$m_\sigma^2 = m^2 - c + 3\left(\lambda_1 + \frac{\lambda_2}{2}\right)\bar{\sigma}^2, \tag{8}$$

$$m_{a_0}^2 = m^2 + c + \left(\lambda_1 + \frac{3\lambda_2}{2}\right)\bar{\sigma}^2, \tag{9}$$

$$m_\eta^2 = m^2 + c + \left(\lambda_1 + \frac{\lambda_2}{2}\right)\bar{\sigma}^2, \tag{10}$$

$$m_\pi^2 = m^2 - c + \left(\lambda_1 + \frac{\lambda_2}{2}\right)\bar{\sigma}^2, \tag{11}$$

$$m_q = \frac{g\bar{\sigma}}{2}. \tag{12}$$

Using (8)–(12), the parameters of the Lagrangian (3) are obtained as

$$\lambda_1 = \frac{m_\sigma^2 + m_\eta^2 - m_{a_0}^2 - m_\pi^2}{2\bar{\sigma}^2}, \tag{13}$$

$$\lambda_2 = \frac{m_{a_0}^2 - m_\eta^2}{\bar{\sigma}^2}, \tag{14}$$

$$m^2 = m_\pi^2 + \frac{m_\eta^2 - m_\sigma^2}{2}, \tag{15}$$

$$c = \frac{m_\eta^2 - m_\pi^2}{2}, \tag{16}$$

$$\frac{g^2}{4} = \frac{m_q^2}{\bar{\sigma}^2} \tag{17}$$

and the tree-level effective potential is written as

$$U(\bar{\sigma}) = \frac{1}{2}m^2\bar{\sigma}^2 - \frac{1}{2}c\bar{\sigma}^2 + \frac{1}{4}\left(\lambda_1 + \frac{1}{2}\lambda_2\right)\bar{\sigma}^4 - h\bar{\sigma}. \tag{18}$$

The stationarity condition for the effective potential (18) gives

$$h = m_\pi^2 \bar{\sigma}. \tag{19}$$

The minimum of the effective potential at the tree level is given by $\bar{\sigma} = f_\pi$. Here it is pertinent to mention that when one reads the coefficient of $\frac{\bar{\sigma}^2}{2}$ as the one single coefficient $(m^2 - c)$ in which m_η dependence cancels out and the coefficient of $\frac{\bar{\sigma}^4}{4}$ as another single coefficient $(\lambda_1 + \frac{\lambda_2}{2})$ where the m_η and m_{a_0} dependence cancels out, we see that the tree-level effective potential of the $SU_L(2) \times SU_R(2)$ sigma model becomes equivalent to the tree-level potential

of the $O(4)$ sigma model, where the degrees of freedom are σ and π only.

We are considering a spatially uniform thermodynamic system in the equilibrium at temperature T and chemical potential μ_q ($q = u$ and d). The partition function is written as the path integral over the quark/antiquark and meson fields [27,42,46]

$$\begin{aligned}\mathcal{Z} &= \mathrm{Tr}\,\exp[-\beta(\hat{\mathcal{H}} - \mu\hat{\mathcal{N}})] \\ &= \int \mathcal{D}\sigma\mathcal{D}\vec{a}_0\mathcal{D}\eta\mathcal{D}\vec{\pi}\int \mathcal{D}\psi\mathcal{D}\overline{\psi}\exp\left[-\int_0^\beta d\tau\int_V d^3x\right. \\ &\quad\left.\times\left(\mathcal{L}^{\mathcal{E}}_{\mathcal{QM}} + \sum_{q=u,d}\mu\bar{q}\gamma^0 q\right)\right],\end{aligned} \tag{20}$$

where V is the volume of the system, $\beta = \frac{1}{T}$, and the superscript $\mathcal{E}$ denotes the Euclidean Lagrangian. In this paper,we assume that the masses of u and d quarks are equal in magnitude. Thus the quark chemical potential of the u and d quarks become equal, i.e., $\mu = \mu_u = \mu_d$. We evaluate the partition function in the mean field approximation. We replace the meson fields by their expectation value $\langle\mathcal{M}\rangle = t_0\bar{\sigma}$ and neglect both the thermal and quantum fluctuations of the meson fields, while the quarks and antiquarks are retained as quantum fields.

In the mean-field approximation, the thermodynamic grand potential for the QM model is given as

$$\begin{aligned}\Omega_{\mathrm{MF}}(T,\mu;\bar{\sigma}) &= -T\frac{\ln\mathcal{Z}}{V} \\ &= U(\bar{\sigma}) + \Omega_{q\bar{q}}(T,\mu;\bar{\sigma}).\end{aligned} \tag{21}$$

The quark/antiquark contribution is given by

$$\Omega_{q\bar{q}}(T,\mu;\bar{\sigma}) = \Omega^{\mathrm{vac}}_{q\bar{q}} + \Omega^{T,\mu}_{q\bar{q}} \tag{22}$$

$$\Omega^{\mathrm{vac}}_{q\bar{q}} = -2N_c\sum_q\int\frac{d^3p}{(2\pi)^3}E_q\theta(\Lambda_c^2 - \vec{p}^2) \tag{23}$$

$$\begin{aligned}\Omega^{T,\mu}_{q\bar{q}} &= -2N_c\sum_q\int\frac{d^3p}{(2\pi)^3}T[\ln(1+e^{-E_q^+/T}) \\ &\quad + \ln(1+e^{-E_q^-/T})].\end{aligned} \tag{24}$$

The first term of Eq. (22) denotes the fermion vacuum contribution, where Λ_c is the ultraviolet cutoff. $\mathrm{E}_q^{\pm} = E_q \mp \mu$ and $E_q = \sqrt{p^2 + {m_q}^2}$ is the flavor dependent single particle energy of quark/antiquark, $m_q = \frac{g\bar{\sigma}}{2}$ is the mass of the given quark flavor.

Neglecting the quark one-loop vacuum term of Eq. (22) in the standard mean-field approximation (S-MFA), the QM model grand potential is written as

$$\begin{aligned}\Omega_{QM}(\bar{\sigma},T,\mu) &= U(\bar{\sigma}) + \Omega^{T,\mu}_{q\bar{q}} \\ \frac{\partial\Omega_{QM}(\bar{\sigma},T,\mu)}{\partial\bar{\sigma}} &= 0.\end{aligned} \tag{25}$$

The global minima of the grand potential in Eq. (25) gives the chiral condensate as a function of the temperature T and the chemical potential μ.

III. QM MODEL WITH VACUUM TERM

We will describe the calculation of the effective potential when the quark one-loop vacuum divergence of Eq. (22) is properly regularized using the minimal subtraction scheme. Here the σ and π meson curvature mass (screening mass), defined by the second derivative of the thermodynamic potential at its minimum, has been used for fixing the model parameters. The zero temperature quark one-loop vacuum contribution is written as

$$\Omega^{\mathrm{vac}}_{q\bar{q}} = -2N_c\sum_q\int\frac{d^3p}{(2\pi)^3}E_q. \tag{26}$$

When Eq. (26) is dimensionally regularized near three dimensions, $d = 3 - 2\epsilon$, one gets the ϵ zeroth order potential as

$$\Omega^{\mathrm{vac}}_{q\bar{q}} = \frac{N_c}{(4\pi)^2}\sum_q m_q^4\left[\frac{1}{\epsilon} + \frac{3}{2} + \ln(4\pi e^{-\gamma_E}) + \ln\left(\frac{\Lambda^2}{m_q^2}\right)\right]. \tag{27}$$

Redefining $\Lambda^2 \to \Lambda^2\frac{e^{\gamma_E}}{4\pi}$ in Eq. (27), one gets

$$\Omega^{\mathrm{vac}}_{q\bar{q}} = \frac{N_c}{(4\pi)^2}\sum_q m_q^4\left[\frac{1}{\epsilon} + \frac{3}{2} + \ln\left(\frac{\Lambda^2}{m_q^2}\right)\right], \tag{28}$$

where Λ is the renormalization scale.

The thermodynamic potential is renormalized by adding the following counterterm to the Lagrangian of the QM model:

$$\delta\mathcal{L} = \frac{N_c}{(4\pi)^2}\sum_q\frac{m_q^4}{\epsilon}. \tag{29}$$

Now the first term of Eq. (22) is replaced by the appropriately renormalized quark one-loop vacuum contribution of Eq. (27):

$$\Omega^{\mathrm{vac}}_{q\bar{q}} = \frac{N_c}{(4\pi)^2}\sum_q m_q^4\left[\frac{3}{2} + \ln\left(\frac{\Lambda^2}{m_q^2}\right)\right]. \tag{30}$$

Since the vacuum ($\mu = 0$ and $T = 0$) grand potential gets contributions from $U(\bar{\sigma})$ and $\Omega^{\mathrm{vac}}_{q\bar{q}}$, it becomes renormalization scale dependent:

$$\Omega^{\Lambda}(\bar{\sigma}) = U(\bar{\sigma}) + \Omega^{\rm vac}_{q\bar{q}}. \tag{31}$$

The unknown model parameters m^2, c, λ_1, λ_2 and h are obtained using the meson curvature masses in which the contribution from the vacuum quark fluctuations have also been taken into account. The details of the model parameter determination are presented in Appendix A.

When the calculated model parameters get substituted in the expression of $U(\bar{\sigma})$, one can rewrite Eq. (31) as

$$\begin{aligned}\Omega^{\Lambda}(\bar{\sigma}) =& \frac{1}{2}\left(m_s^2 - \frac{N_c g^4 f_\pi^2}{2(4\pi)^2}\right)\bar{\sigma}^2 - \frac{1}{2}c\bar{\sigma}^2 \\ &+ \frac{1}{4}\left(\lambda_1 + \frac{\lambda_{2s}}{2} - \frac{N_c g^4}{2(4\pi)^2}\ln\left(\frac{4\Lambda^2}{g^2 f_\pi^2}\right)\right)\bar{\sigma}^4 - h\bar{\sigma} \\ &+ \frac{N_c g^4 \bar{\sigma}^4}{8(4\pi)^2}\left[\frac{3}{2} + \ln\left(\frac{\Lambda^2}{m_q^2}\right)\right].\end{aligned} \tag{32}$$

After the rearrangement of terms, we find the complete cancellation of renormalization scale Λ in the vacuum grand potential. It is recast as

$$\begin{aligned}\Omega(\bar{\sigma}) =& \frac{1}{2}\left(m_s^2 - \frac{N_c g^4 f_\pi^2}{2(4\pi)^2}\right)\bar{\sigma}^2 - \frac{1}{2}c\bar{\sigma}^2 \\ &+ \frac{1}{4}\left(\lambda_1 + \frac{\lambda_{2s}}{2} + \frac{3N_c g^4}{4(4\pi)^2}\right)\bar{\sigma}^4 - h\bar{\sigma} + \frac{N_c g^4 \bar{\sigma}^4}{8(4\pi)^2}\ln\left(\frac{f_\pi^2}{\bar{\sigma}^2}\right).\end{aligned} \tag{33}$$

Now, in the presence of appropriately renormalized quark one-loop vacuum contribution, the thermodynamic grand potential of the quark-meson model with vacuum term (QMVT) will be written as

$$\Omega_{\rm QMVT}((\bar{\sigma}, T, \mu)) = \Omega(\bar{\sigma}) + \Omega^{T,\mu}_{q\bar{q}} \tag{34}$$

$$\frac{\partial \Omega_{\rm QMVT}(\bar{\sigma}, T, \mu)}{\partial \bar{\sigma}} = 0. \tag{35}$$

The global minima of the grand potential in Eq. (35) gives the PQMVT model chiral condensate $\bar{\sigma}$ as a function of the temperature T and the chemical potential μ. We point out that here for $T = 0$ the stationarity condition $\frac{\partial \Omega(\bar{\sigma})}{\partial \bar{\sigma}}$ gives $h = m_\pi^2 \bar{\sigma}$. In this scheme of parameters fixing, the dressing of the meson propagator is not considered. Therefore the pion decay constant f_π does not get renormalized. The contribution from the vacuum quark fluctuations to the effective potential modifies the parameters in such way that the stationarity condition gives the same result as in Eq. (19). The modified curvature mass of the pion given in Appendix A remains equal to the pion pole mass. Finally the minimum of the effective potential remains at $\bar{\sigma} = f_\pi$.

IV. RENORMALIZED QUARK-MESON MODEL

Several of the relatively recent investigations in the above detailed QMVT model framework have used the standard procedure of equating the vacuum expectation value of the sigma mean field to the pion decay constant. Afterwards the $\sigma, \vec{a_0}, \vec{\pi}$ and η meson masses are put equal to their curvature (or screening) masses [50–63]. However, in principle, the physical masses of the mesons are given by the pole of their propagators. Also, the residue of the pion propagator at its pole gets related to the pion decay constant [66–68]. Furthermore, since the effective potential is the generator of the n-point functions of the theory at zero external momenta, the curvature masses are equivalent to defining the meson masses using the evaluation of self-energy at zero momentum [64,65,69,70]. It has been emphasized that the pole definition is the physical and gauge invariant one [72,73]. The curvature mass prescription is equivalent to the pole mass prescription for the parameter fixing of the model in the absence of Dirac sea contributions but when the one quark loop vacuum correction is incorporated, the screening masses of mesons start to differ from the pole masses [66,68]. In view of the above considerations, it becomes necessary to use the following detailed description of the exact on-shell parameter fixing procedure for the renormalized quark-meson (RQM) model. Here the physical (pole) masses of the mesons and the pion decay constant are put into the relation of the running mass parameter and couplings by using the on-shell and the minimal subtraction renormalization schemes [69,71].

A. Self-energies and counterterms

Once quark one-loop corrections are taken into account, the tree-level parameters of Eqs. (13)–(17) become inconsistent unless the on-shell renormalization prescription is used. Though the dimensional regularization is used to regularize the divergent loop integrals in the on-shell scheme, the counterterm choices are different from the minimal subtraction scheme. The loop corrections to the self-energies are canceled exactly by the suitable choice of counterterms in the on-shell scheme. The renormalized parameters become renormalization scale independent as couplings are evaluated on shell. The wave functions/fields and parameters of Eq. (1) are bare quantities. The counterterms δm^2, δg^2, $\delta\lambda_1$, $\delta\lambda_2$, δc and δh for the parameters and the counterterms δZ_σ, δZ_{a_0}, δZ_η, δZ_π, δZ_ψ and $\delta Z_{\bar{\sigma}}$ for the wave functions/fields are introduced in the Lagrangian (1) where the renormalized fields and couplings are defined as

$$\sigma_b = \sqrt{Z_\sigma}\sigma, \qquad \eta_b = \sqrt{Z_\eta}\eta, \qquad a^i_{0b} = \sqrt{Z_{a_0}}a_0 \tag{36}$$

$$\pi^i_b = \sqrt{Z_\pi}\pi, \qquad \psi_b = \sqrt{Z_\psi}\psi, \qquad m_b^2 = Z_m m^2 \tag{37}$$

$$\lambda_{1b} = Z_{\lambda_1}\lambda_1, \qquad \lambda_{2b} = Z_{\lambda_2}\lambda_2, \qquad g_b = \sqrt{Z_g}g \tag{38}$$

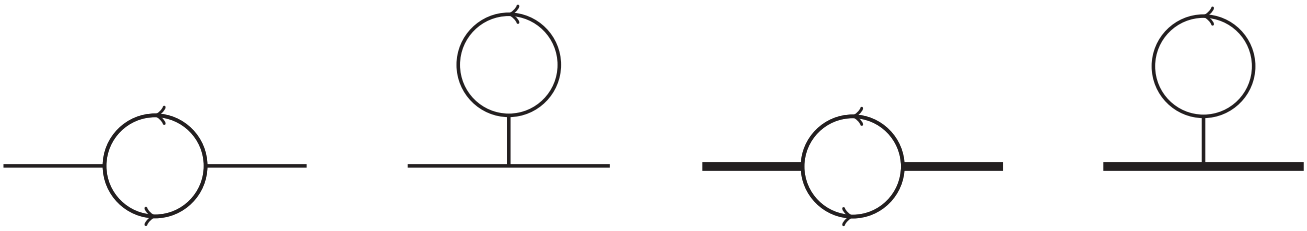

(a) (b)

FIG. 1. (a) One loop self-energy diagrams for sigma particle. (b) One loop self-energy diagrams for the a_0.

$$h_b = Z_h h, \qquad c_b = Z_c c, \qquad \bar{\sigma}_b = \sqrt{Z_{\bar{\sigma}}}\bar{\sigma}, \quad (39)$$

where the $Z_{(\sigma,a_0,\eta,\pi,\psi,\bar{\sigma})} = 1 + \delta Z_{(\sigma,a_0,\eta,\pi,\psi,\bar{\sigma})}$ denote the field strength renormalization constant while $Z_{(m,\lambda_1,\lambda_2,g,h,c)} = 1 + \delta Z_{(m,\lambda_1,\lambda_2,g,h,c)}$ denote the mass and coupling renormalization constant. Following Refs. [65,69–71], counterterms δm^2, $\delta\lambda_1$, $\delta\lambda_2$, δc and δg^2, δh can be expressed in terms of the counterterms δm_σ^2, $\delta m_{a_0}^2$, δm_η^2, δm_π^2 and δm_q, $\delta\bar{\sigma}^2$. Using Eqs. (8)–(12) together with Eqs. (36)–(39), we can write

$$\delta\lambda_1 = \frac{\delta m_\sigma^2 + \delta m_\eta^2 - \delta m_{a_0}^2 - \delta m_\pi^2}{2\bar{\sigma}^2} - \lambda_1 \frac{\delta\bar{\sigma}^2}{\bar{\sigma}^2} \quad (40)$$

$$\delta\lambda_2 = \frac{\delta m_{a_0}^2 - \delta m_\eta^2}{\bar{\sigma}^2} - \lambda_2 \frac{\delta\bar{\sigma}^2}{\bar{\sigma}^2} \quad (41)$$

$$\delta c = \frac{\delta m_\eta^2 - \delta m_\pi^2}{2} \quad (42)$$

$$\delta m^2 = \delta m_\pi^2 + \frac{\delta m_\eta^2 - \delta m_\sigma^2}{2} \quad (43)$$

$$\frac{\delta g^2}{4} = \frac{\delta m_q^2}{\bar{\sigma}^2} - g^2 \frac{\delta\bar{\sigma}^2}{4\bar{\sigma}^2}. \quad (44)$$

In the large N_c limit, the one-loop correction to the quark field and the quark mass is zero because the π and σ loops that may renormalize the quark propagator are of order N_c^0. Hence $Z_\psi = 1$ and the quark self-energy correction $\delta m_q = 0$. The one-loop correction at the pion-quark $\pi\bar{\psi}\psi$ vertex is also of order N_c^0, hence get neglected. In consequence, we get $Z_\psi\sqrt{Z_g g^2}\sqrt{Z_\pi} \approx g(1 + \frac{1}{2}\frac{\delta g^2}{g^2} + \frac{1}{2}\delta Z_\pi) = g$. Thus $\frac{\delta g^2}{g^2} + \delta Z_\pi = 0$. Furthermore the $\delta m_q = 0$ implies that $\delta g\bar{\sigma}/2 + g\delta\bar{\sigma}/2 = 0$. Equation (44) gives

$$\frac{\delta\bar{\sigma}^2}{\bar{\sigma}^2} = -\frac{\delta g^2}{g^2} = \delta Z_\pi. \quad (45)$$

Now one can rewrite Eqs. (40) and (41) as

$$\delta\lambda_1 = \frac{\delta m_\sigma^2 + \delta m_\eta^2 - \delta m_{a_0}^2 - \delta m_\pi^2}{2\bar{\sigma}^2} - \lambda_1\delta Z_\pi \quad (46)$$

$$\delta\lambda_2 = \frac{\delta m_{a_0}^2 - \delta m_\eta^2}{\bar{\sigma}^2} - \lambda_2\delta Z_\pi. \quad (47)$$

The Feynman diagrams for the meson self-energies are drawn in the figures. The scalar σ and a_0 mesons are represented by a solid line and a thick solid line respectively in Figs. 1(a) and 1(b) where an arrow on the solid line denotes a quark. The corresponding self-energy expressions for the σ and a_0^i are written as

$$\Sigma_\sigma(p^2) = -\frac{2N_c g^2}{(4\pi)^2}\left[\mathcal{A}(m_q^2) - \frac{1}{2}(p^2 - 4m_q^2)\mathcal{B}(p^2)\right] + \frac{24(\lambda_1 + \frac{\lambda_2}{2})g\bar{\sigma}N_c m_q}{m_\sigma^2}\mathcal{A}(m_q^2), \quad (48)$$

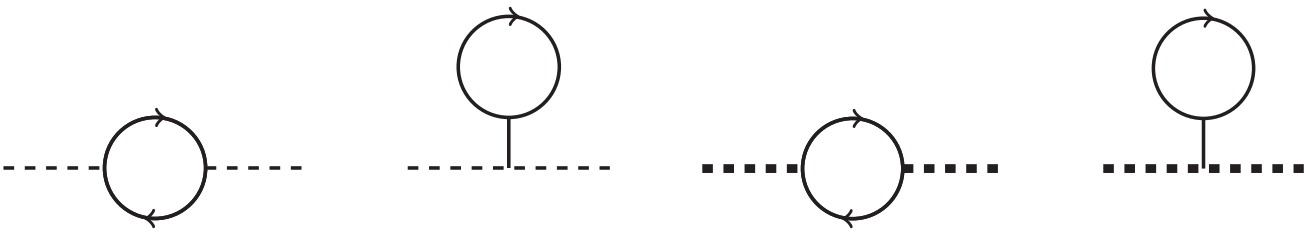

(a) (b)

FIG. 2. (a) One-loop self-energy diagrams for the eta. (b) One-loop self-energy diagrams for the pion.

$$\Sigma_{a_0}(p^2) = -\frac{2N_c g^2}{(4\pi)^2}\left[\mathcal{A}(m_q^2) - \frac{1}{2}(p^2 - 4m_q^2)\mathcal{B}(p^2)\right] + \frac{8(\lambda_1 + \frac{3\lambda_2}{2})g\bar{\sigma}N_c m_q}{m_\sigma^2}\mathcal{A}(m_q^2). \quad (49)$$

The pseudoscalar η and π_0^i mesons in Figs. 2(a) and 2(b) are drawn by a dashed line and a thick dashed line in respective order. The corresponding self-energy expressions for η and π_0^i are given by

$$\Sigma_\eta(p^2) = -\frac{2N_c g^2}{(4\pi)^2}\left[\mathcal{A}(m_q^2) - \frac{1}{2}p^2\mathcal{B}(p^2)\right] + \frac{8(\lambda_1 + \frac{\lambda_2}{2})g\bar{\sigma}N_c m_q}{m_\sigma^2}\mathcal{A}(m_q^2). \quad (50)$$

$$\Sigma_\pi(p^2) = -\frac{2N_c g^2}{(4\pi)^2}\left[\mathcal{A}(m_q^2) - \frac{1}{2}p^2\mathcal{B}(p^2)\right] + \frac{8(\lambda_1 + \frac{\lambda_2}{2})g\bar{\sigma}N_c m_q}{m_\sigma^2}\mathcal{A}(m_q^2), \quad (51)$$

where $\mathcal{A}(m_q^2)$ and $\mathcal{B}(p^2)$ are defined in Appendix B and the last terms of Eqs. (48)–(51) are the contributions of the tadpole diagrams to the self-energies. The counterterm diagrams for the two-point functions of the scalar mesons σ, $\mathbf{a_0}$ and the pseudoscalar mesons η, π are shown respectively in Figs. 3 and 4.

FIG. 3. Counterterm for the two-point functions of the scalar σ and $\mathbf{a_0}$ meson.

FIG. 4. Counterterm for the two-point functions of the pseudoscalar η and π meson.

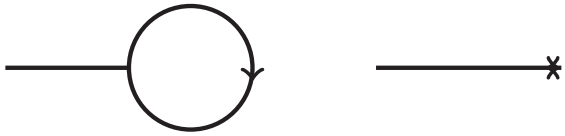

FIG. 5. One-point diagram for the sigma particle and its counterterm.

The diagram for the quark one-loop correction to the one-point function and its counterterm diagram is shown in Fig. 5. It can be written as

$$\delta\Gamma^{(1)} = -4N_c g m_q \mathcal{A}(m_q^2) + i\delta t. \quad (52)$$

B. Parameters with renormalization

The vanishing of the one-point function $\Gamma^{(1)} = it = i(h - m_\pi^2\bar{\sigma})$ gives the tree-level equation of motion $t = 0$ and fixes the classical minimum of the effective potential. The first renormalization condition $\langle\sigma\rangle = 0$ requires that the one-loop correction $\delta\Gamma^{(1)}$ to the one point function is put to zero such that the minimum of the effective potential does not change. Thus the first renormalization condition $\delta\Gamma^{(1)} = 0$ gives

$$\delta t = -4iN_c g m_q \mathcal{A}(m_q^2). \quad (53)$$

The equation $h = t + m_\pi^2\bar{\sigma}$ enables the writing of the counterterm δh in terms of the tadpole counterterm δt:

$$\delta h = m_\pi^2\delta\bar{\sigma} + \delta m_\pi^2\bar{\sigma} + \delta t. \quad (54)$$

Using Eq. (45) we can write

$$\delta h = \frac{1}{2}m_\pi^2\bar{\sigma}\delta Z_\pi + \delta m_\pi^2\bar{\sigma} + \delta t. \quad (55)$$

We can write the inverse propagator for the scalar σ, a_0 and pseudoscalar π, η mesons as

$$p^2 - m_{\sigma,a_0,\pi,\eta}^2 - i\Sigma_{\sigma,a_0,\pi,\eta}(p^2) + \text{counterterms}. \quad (56)$$

The renormalized mass in the Lagrangian is put equal to the physical mass, i.e., $m = m_{\text{pole}}$[1] when the on-shell scheme gets implemented and we can write

$$\Sigma(p^2 = m_{\sigma,a_0,\pi,\eta}^2) + \text{counterterms} = 0. \quad (57)$$

Since the propagator residue is put to unity in the on-shell scheme, one gets

[1]The contribution of the imaginary parts of the self-energies into defining the mass has not been considered.

$$\frac{\partial}{\partial p^2}\Sigma_{\sigma,a_0,\pi,\eta}(p^2)|_{p^2=m^2_{\sigma,a_0,\pi,\eta}} + \text{counterterms} = 0. \quad (58)$$

Figures 3 and 4 show diagrams for the counterterms of the two-point functions of the scalar σ, a_0 and pseudoscalar π, η mesons are written as

$$\Sigma^{\text{ct1}}_{\sigma}(p^2) = i[\delta Z_\sigma(p^2 - m^2_\sigma) - \delta m^2_\sigma], \quad (59)$$

$$\Sigma^{\text{ct1}}_{a_0}(p^2) = i[\delta Z_{a_0}(p^2 - m^2_{a_0}) - \delta m^2_{a_0}], \quad (60)$$

$$\Sigma^{\text{ct1}}_{\pi}(p^2) = i[\delta Z_\pi(p^2 - m^2_\pi) - \delta m^2_\pi], \quad (61)$$

$$\Sigma^{\text{ct1}}_{\eta}(p^2) = i[\delta Z_\eta(p^2 - m^2_\eta) - \delta m^2_\eta], \quad (62)$$

$$\Sigma^{\text{ct2}}_{\sigma} = 3\Sigma^{\text{ct2}}_{\pi} = 3\Sigma^{\text{ct2}}_{\eta}, \quad (63)$$

$$= -\frac{24(\lambda_1 + \frac{\lambda_2}{2})g\bar{\sigma}N_c m_q}{m^2_\sigma}\mathcal{A}(m^2_q), \quad (64)$$

$$\Sigma^{\text{ct2}}_{a_0} = -\frac{8(\lambda_1 + \frac{3\lambda_2}{2})g\bar{\sigma}N_c m_q}{m^2_\sigma}\mathcal{A}(m^2_q). \quad (65)$$

The counterterms of Eq. (63) completely cancel the respective tadpole contributions to the self-energies of σ, a_0 and π, η. The evaluation of the self-energies and their derivatives in on-shell conditions give all the renormalization constants. When Eqs. (57), (58), and (59)–(62) are combined, we obtain the following set of equations:

$$\delta m^2_\sigma = -i\Sigma_\sigma(m^2_\sigma); \qquad \delta Z_\sigma = i\frac{\partial}{\partial p^2}\Sigma_\sigma(p^2)|_{p^2=m^2_\sigma}, \quad (66)$$

$$\delta m^2_{a_0} = -i\Sigma_{a_0}(m^2_{a_0}); \quad \delta Z_{a_0} = i\frac{\partial}{\partial p^2}\Sigma_{a_0}(p^2)|_{p^2=m^2_{a_0}}, \quad (67)$$

$$\delta m^2_\pi = -i\Sigma_\pi(m^2_\pi); \qquad \delta Z_\pi = i\frac{\partial}{\partial p^2}\Sigma_\pi(p^2)|_{p^2=m^2_\pi}, \quad (68)$$

$$\delta m^2_\eta = -i\Sigma_\eta(m^2_\eta); \qquad \delta Z_\eta = i\frac{\partial}{\partial p^2}\Sigma_\eta(p^2)|_{p^2=m^2_\eta}. \quad (69)$$

When the self-energy (neglecting the tadpole contributions) expressions from Eqs. (48)–(51) are used, we get the following equations:

$$\delta m^2_\sigma = 2ig^2N_c\left[\mathcal{A}(m^2_q) - \frac{1}{2}(m^2_\sigma - 4m^2_q)\mathcal{B}(m^2_\sigma)\right], \quad (70)$$

$$\delta m^2_{a_0} = 2ig^2N_c\left[\mathcal{A}(m^2_q) - \frac{1}{2}(m^2_{a_0} - 4m^2_q)\mathcal{B}(m^2_{a_0})\right], \quad (71)$$

$$\delta m^2_\pi = 2ig^2N_c\left[\mathcal{A}(m^2_q) - \frac{1}{2}m^2_\pi\mathcal{B}(m^2_\pi)\right], \quad (72)$$

$$\delta m^2_\eta = 2ig^2N_c\left[\mathcal{A}(m^2_q) - \frac{1}{2}m^2_\eta\mathcal{B}(m^2_\eta)\right], \quad (73)$$

$$\delta Z_\sigma = ig^2N_c[\mathcal{B}(m^2_\sigma) + (m^2_\sigma - 4m^2_q)\mathcal{B}'(m^2_\sigma)], \quad (74)$$

$$\delta Z_{a_0} = ig^2N_c[\mathcal{B}(m^2_{a_0}) + (m^2_{a_0} - 4m^2_q)\mathcal{B}'(m^2_{a_0})], \quad (75)$$

$$\delta Z_\pi = ig^2N_c[\mathcal{B}(m^2_\pi) + m^2_\pi\mathcal{B}'(m^2_\pi)], \quad (76)$$

$$\delta Z_\eta = ig^2N_c[\mathcal{B}(m^2_\eta) + m^2_\eta\mathcal{B}'(m^2_\eta)]. \quad (77)$$

Exploiting Eqs. (70)–(77) together with Eqs. (40)–(45) and (55), we find the following expressions for the counterterms in the on-shell scheme:

$$\begin{aligned}\delta\lambda_{1\text{OS}} &= \frac{iN_cg^2}{\bar{\sigma}^2}\left[-\frac{1}{2}(m^2_\sigma - 4m^2_q)\mathcal{B}(m^2_\sigma) - \frac{1}{2}m^2_\eta\mathcal{B}(m^2_\eta) + \frac{1}{2}(m^2_{a_0} - 4m^2_q)\mathcal{B}(m^2_{a_0}) + \frac{1}{2}m^2_\pi\mathcal{B}(m^2_\pi)\right] - \lambda_1 ig^2N_c[\mathcal{B}(m^2_\pi) + m^2_\pi\mathcal{B}'(m^2_\pi)] \\ &= \delta\lambda_{1\text{div}} + 2\lambda_1\frac{N_cg^2}{(4\pi)^2}\ln\left(\frac{\Lambda^2}{m^2_q}\right) + \frac{N_cg^2}{(4\pi)^2}\left[\frac{(m^2_\sigma - 4m^2_q)\mathcal{C}(m^2_\sigma) + m^2_\eta\mathcal{C}(m^2_\eta) - (m^2_{a_0} - 4m^2_q)\mathcal{C}(m^2_{a_0}) - m^2_\pi\mathcal{C}(m^2_\pi)}{2\bar{\sigma}^2}\right. \\ &\quad \left. + \lambda_1(\mathcal{C}(m^2_\pi) + m^2_\pi\mathcal{C}'(m^2_\pi))\right], \end{aligned} \quad (78)$$

$$\begin{aligned}\delta\lambda_{2\text{OS}} &= \frac{iN_cg^2}{\bar{\sigma}^2}[-(m^2_{a_0} - 4m^2_q)\mathcal{B}(m^2_{a_0}) + m^2_\eta\mathcal{B}(m^2_\eta)] - \lambda_2 ig^2N_c[\mathcal{B}(m^2_\pi) + m^2_\pi\mathcal{B}'(m^2_\pi)], \\ &= \delta\lambda_{2\text{div}} + \frac{N_cg^2}{(4\pi)^2}(2\lambda_2 - g^2)\ln\left(\frac{\Lambda^2}{m^2_q}\right) \\ &\quad + \frac{N_cg^2}{(4\pi)^2}\left[\frac{(m^2_{a_0} - 4m^2_q)\mathcal{C}(m^2_{a_0}) - m^2_\eta\mathcal{C}(m^2_\eta)}{\bar{\sigma}^2} + \lambda_2(m^2_\pi\mathcal{C}'(m^2_\pi) + \mathcal{C}(m^2_\pi))\right], \end{aligned} \quad (79)$$

$$\delta m^2_{\rm OS} = 2iN_c g^2\left[\mathcal{A}(m_q^2) - \frac{1}{2}m_\pi^2\mathcal{B}(m_\pi^2)\right] + iN_c g^2\left[-\frac{1}{2}m_\eta^2\mathcal{B}(m_\eta^2) + \frac{1}{2}(m_\sigma^2 - 4m_q^2)\mathcal{B}(m_\sigma^2)\right]$$
$$= \delta m^2_{\rm div} + \frac{N_c g^2}{(4\pi)^2}m^2\ln\left(\frac{\Lambda^2}{m_q^2}\right) + \frac{N_c g^2}{(4\pi)^2}\left[m_\pi^2\mathcal{C}(m_\pi^2) + \frac{m_\eta^2\mathcal{C}(m_\eta^2) - (m_\sigma^2 - 4m_q^2)\mathcal{C}(m_\sigma^2)}{2} - 2m_q^2\right], \tag{80}$$

$$\delta c_{\rm OS} = \frac{iN_c g^2}{2}[-m_\eta^2\mathcal{B}(m_\eta^2) + m_\pi^2\mathcal{B}(m_\pi^2)]$$
$$= \delta c_{\rm div} + \frac{N_c g^2}{(4\pi)^2}c\ln\left(\frac{\Lambda^2}{m_q^2}\right) + \frac{N_c g^2}{2(4\pi)^2}[m_\eta^2\mathcal{C}(m_\eta^2) - m_\pi^2\mathcal{C}(m_\pi^2)], \tag{81}$$

$$\delta g^2_{\rm OS} = -iN_c g^4[m_\pi^2\mathcal{B}'(m_\pi^2) + \mathcal{B}(m_\pi^2)]$$
$$= \delta g^2_{\rm div} + \frac{N_c g^4}{(4\pi)^2}\left[\ln\left(\frac{\Lambda^2}{m_q^2}\right) + \mathcal{C}(m_\pi^2) + m_\pi^2\mathcal{C}'(m_\pi^2)\right], \tag{82}$$

$$\delta h_{\rm OS} = \frac{iN_c g^2}{2(4\pi)^2}h[m_\pi^2\mathcal{B}'(m_\pi^2) - \mathcal{B}(m_\pi^2)]$$
$$= \delta h_{\rm div} + \frac{N_c g^2}{2(4\pi)^2}h\left[\ln\left(\frac{\Lambda^2}{m_q^2}\right) + \mathcal{C}(m_\pi^2) - m_\pi^2\mathcal{C}'(m_\pi^2)\right] \tag{83}$$

$$\delta\bar{\sigma}^2_{\rm OS} = iN_c g^2\bar{\sigma}^2[m_\pi^2\mathcal{B}'(m_\pi^2) + \mathcal{B}(m_\pi^2)]$$
$$= \delta\bar{\sigma}^2_{\rm div} - \frac{N_c g^2\bar{\sigma}^2}{(4\pi)^2}\left[\ln\left(\frac{\Lambda^2}{m_q^2}\right) + \mathcal{C}(m_\pi^2) + m_\pi^2\mathcal{C}'(m_\pi^2)\right] \tag{84}$$

$$\delta Z_\sigma^{\rm OS} = \delta Z_{\sigma,\rm div} - \frac{N_c g^2}{(4\pi)^2}\left[\ln\left(\frac{\Lambda^2}{m_q^2}\right) + \mathcal{C}(m_\sigma^2) + (m_\sigma^2 - 4m_q^2)\mathcal{C}'(m_\sigma^2)\right] \tag{85}$$

$$\delta Z_{a_0}^{\rm OS} = \delta Z_{a_0,\rm div} - \frac{N_c g^2}{(4\pi)^2}\left[\ln\left(\frac{\Lambda^2}{m_q^2}\right) + \mathcal{C}(m_{a_0}^2) + (m_{a_0}^2 - 4m_q^2)\mathcal{C}'(m_{a_0}^2)\right] \tag{86}$$

$$\delta Z_\pi^{\rm OS} = \delta Z_{\pi,\rm div} - \frac{N_c g^2}{(4\pi)^2}\left[\ln\left(\frac{\Lambda^2}{m_q^2}\right) + \mathcal{C}(m_\pi^2) + m_\pi^2\mathcal{C}'(m_\pi^2)\right] \tag{87}$$

$$\delta Z_\eta^{\rm OS} = \delta Z_{\eta,\rm div} - \frac{N_c g^2}{(4\pi)^2}\left[\ln\left(\frac{\Lambda^2}{m_q^2}\right) + \mathcal{C}(m_\eta^2) + m_\eta^2\mathcal{C}'(m_\eta^2)\right]. \tag{88}$$

Here, λ_1, λ_2, m^2, c, h, and g^2 in Eqs. (78)–(84) are the same as in Eqs. (13)–(17) and (19) for the QM model with the "no Dirac sea" approximation.

The $\mathcal{B}(m^2), \mathcal{B}'(m^2)$ and $\mathcal{C}(m^2), \mathcal{C}'(m^2)$ are defined in Appendix B. The divergent parts of the counterterms are $\delta\lambda_{1\rm div} = \frac{N_c g^2 2\lambda_1}{(4\pi)^2\epsilon}$, $\delta\lambda_{2\rm div} = \frac{N_c g^2}{(4\pi)^2\epsilon}(2\lambda_2 - g^2)$, $\delta m^2_{\rm div} = \frac{N_c g^2 m^2}{(4\pi)^2\epsilon}$, $\delta c_{\rm div} = \frac{N_c g^2 c}{(4\pi)^2\epsilon}$, $\delta g^2_{\rm div} = \frac{N_c g^4}{(4\pi)^2\epsilon}$, $\delta\bar{\sigma}^2_{\rm div} = -\frac{N_c g^2\bar{\sigma}^2}{(4\pi)^2\epsilon}$, $\delta h_{\rm div} = \frac{N_c g^2 h}{2(4\pi)^2\epsilon}$, $\delta Z_{\sigma,\rm div} = \delta Z_{a_0,\rm div} = \delta Z_{\pi,\rm div} = \delta Z_{\eta,\rm div} = -\frac{N_c g^2}{(4\pi)^2\epsilon}$. For both the on-shell and the $\overline{\rm MS}$ schemes, the divergent parts of the counterterms are the same, i.e., $\delta\lambda_{1\rm div} = \delta\lambda_{1\overline{\rm MS}}$, $\delta\lambda_{2\rm div} = \delta\lambda_{2\overline{\rm MS}}$ etc.

Since the bare parameters are independent of the renormalization scheme, we can immediately write down the relations between the renormalized parameters in the on-shell and MS schemes as follows:

$$\lambda_{1\overline{\rm MS}} = \lambda_1 + \delta\lambda_{1\rm OS} - \delta\lambda_{1\overline{\rm MS}} \tag{89}$$

$$\lambda_{2\overline{\rm MS}} = \lambda_2 + \delta\lambda_{2\rm OS} - \delta\lambda_{2\overline{\rm MS}} \tag{90}$$

$$m^2_{\overline{\rm MS}} = m^2 + \delta m^2_{\rm OS} - \delta m^2_{\overline{\rm MS}} \tag{91}$$

$$c_{\overline{\rm MS}} = c + \delta c_{\rm OS} - \delta c_{\overline{\rm MS}} \tag{92}$$

$$h_{\overline{\rm MS}} = h + \delta h_{\rm OS} - \delta h_{\overline{\rm MS}} \tag{93}$$

$$g^2_{\overline{\rm MS}} = g^2 + \delta g^2_{\rm OS} - \delta g^2_{\overline{\rm MS}} \tag{94}$$

$$\bar{\sigma}^2_{\overline{\rm MS}} = \bar{\sigma}^2 + \delta\bar{\sigma}^2_{\rm OS} - \delta\bar{\sigma}^2_{\overline{\rm MS}}. \tag{95}$$

The minimum of the effective potential is at $\bar{\sigma} = f_\pi$ and the masses have the measured value in vacuum. Using the above set of equations together with Eqs. (78)–(84), we can write the scale Λ dependent running parameters in the $\overline{\rm MS}$ scheme as the following:

$$\lambda_{1\overline{\rm MS}}(\Lambda) = \lambda_1 + 2\lambda_1 \frac{N_c g^2}{(4\pi)^2}\ln\left(\frac{\Lambda^2}{m_q^2}\right) + \frac{N_c g^2}{(4\pi)^2}\left[\frac{(m_\sigma^2 - 4m_q^2)\mathcal{C}(m_\sigma^2) + m_\eta^2\mathcal{C}(m_\eta^2) - (m_{a_0}^2 - 4m_q^2)\mathcal{C}(m_{a_0}^2) - m_\pi^2\mathcal{C}(m_\pi^2)}{2f_\pi^2} + \lambda_1(\mathcal{C}(m_\pi^2) + m_\pi^2\mathcal{C}'(m_\pi^2))\right], \tag{96}$$

$$\lambda_{2\overline{\rm MS}}(\Lambda) = \lambda_2 + \frac{N_c g^2}{(4\pi)^2}(2\lambda_2 - g^2)\ln\left(\frac{\Lambda^2}{m_q^2}\right) + \frac{N_c g^2}{(4\pi)^2}\left[\frac{(m_{a_0}^2 - 4m_q^2)\mathcal{C}(m_{a_0}^2) - m_\eta^2\mathcal{C}(m_\eta^2)}{f_\pi^2} + \lambda_2(m_\pi^2\mathcal{C}'(m_\pi^2) + \mathcal{C}(m_\pi^2))\right], \tag{97}$$

$$m^2_{\overline{\rm MS}}(\Lambda) = m^2 + \frac{N_c g^2}{(4\pi)^2} m^2 \ln\left(\frac{\Lambda^2}{m_q^2}\right) + \frac{N_c g^2}{(4\pi)^2}\left[m_\pi^2\mathcal{C}(m_\pi^2) + \frac{m_\eta^2\mathcal{C}(m_\eta^2) - (m_\sigma^2 - 4m_q^2)\mathcal{C}(m_\sigma^2)}{2} - 2m_q^2\right], \tag{98}$$

$$c_{\overline{\rm MS}}(\Lambda) = c + \frac{N_c g^2}{(4\pi)^2} c \ln\left(\frac{\Lambda^2}{m_q^2}\right) + \frac{N_c g^2}{2(4\pi)^2}[m_\eta^2\mathcal{C}(m_\eta^2) - m_\pi^2\mathcal{C}(m_\pi^2)], \tag{99}$$

$$h_{\overline{\rm MS}}(\Lambda) = h + \frac{N_c g^2}{2(4\pi)^2} h\left[\ln\left(\frac{\Lambda^2}{m_q^2}\right) + \mathcal{C}(m_\pi^2) - m_\pi^2\mathcal{C}'(m_\pi^2)\right], \tag{100}$$

$$g^2_{\overline{\rm MS}}(\Lambda) = g^2 + \frac{N_c g^4}{(4\pi)^2}\left[\ln\left(\frac{\Lambda^2}{m_q^2}\right) + \mathcal{C}(m_\pi^2) + m_\pi^2\mathcal{C}'(m_\pi^2)\right], \tag{101}$$

$$\bar{\sigma}^2_{\overline{\rm MS}}(\Lambda) = f_\pi^2 - \frac{4N_c m_q^2}{(4\pi)^2}\left[\ln\left(\frac{\Lambda^2}{m_q^2}\right) + \mathcal{C}(m_\pi^2) + m_\pi^2\mathcal{C}'(m_\pi^2)\right]. \tag{102}$$

$\bar{\sigma} = f_\pi$, λ_1, λ_2, m^2, c, h and g^2 in Eqs. (96)–(102) have the same tree-level QM model values that we obtain after putting $\bar{\sigma} = f_\pi$ in Eqs. (13)–(17) and (19). The numerical values of the QM model parameters c, m_2, λ_1, λ_2 and h for $m_\sigma = 400$, 500 and 600 MeV are given in the Table I.

In the large-N_c limit the parameters $\lambda_{1\overline{\rm MS}}$, $\lambda_{2\overline{\rm MS}}$, $m^2_{\overline{\rm MS}}$, $c_{\overline{\rm MS}}$, $h_{\overline{\rm MS}}$, and $g^2_{\overline{\rm MS}}$ are running with the scale Λ and satisfy a set of the following simultaneous renormalization group equations:

$$\frac{d\lambda_{1\overline{\rm MS}}(\Lambda)}{d\ln(\Lambda)} = \frac{4N_c}{(4\pi)^2} g^2_{\overline{\rm MS}}\lambda_{1\overline{\rm MS}}, \tag{103}$$

$$\frac{d\lambda_{2\overline{\rm MS}}(\Lambda)}{d\ln(\Lambda)} = \frac{2N_c}{(4\pi)^2}[2\lambda_{2\overline{\rm MS}} g^2_{\overline{\rm MS}} - g^4_{\overline{\rm MS}}], \tag{104}$$

$$\frac{dm^2_{\overline{\rm MS}}(\Lambda)}{d\ln(\Lambda)} = \frac{2N_c}{(4\pi)^2} g^2_{\overline{\rm MS}} m^2_{\overline{\rm MS}}, \tag{105}$$

$$\frac{dc_{\overline{\rm MS}}(\Lambda)}{d\ln(\Lambda)} = \frac{2N_c}{(4\pi)^2} g^2_{\overline{\rm MS}} c_{\overline{\rm MS}}, \tag{106}$$

$$\frac{dh_{\overline{\rm MS}}(\Lambda)}{d\ln(\Lambda)} = \frac{N_c}{(4\pi)^2} g^2_{\overline{\rm MS}} h_{\overline{\rm MS}}, \tag{107}$$

$$\frac{dg^2_{\overline{\rm MS}}}{d\ln(\Lambda)} = \frac{2N_c}{(4\pi)^2} g^4_{\overline{\rm MS}}, \tag{108}$$

$$\frac{d\bar{\sigma}^2_{\overline{\rm MS}}}{d\ln(\Lambda)} = -\frac{2N_c}{(4\pi)^2} g^2_{\overline{\rm MS}}\bar{\sigma}^2_{\overline{\rm MS}}. \tag{109}$$

Solving the differential Eqs. (103)–(108), we get the following solutions:

TABLE I. Parameters of the QM model for $m_\sigma = 400$, 500, and 600 MeV.

m_σ (MeV)	c (MeV^2)	m^2 (MeV^2)	λ_1	λ_2	h (MeV^3)
400	$(374.28)^2$	$(297.74)^2$	−30.61	77.51	$(120.99)^3$
500	$(374.28)^2$	$(208.92)^2$	−23.32	77.51	$(120.99)^3$
600	$(374.28)^2$	$-(106.54)^2$	−19.05	77.51	$(120.99)^3$

$$\lambda_{1\overline{\rm MS}}(\Lambda) = \frac{\lambda_{10}}{\left(1-\frac{N_c g_0^2}{(4\pi)^2}\ln\left(\frac{\Lambda^2}{\Lambda_0^2}\right)\right)^2}, \tag{110}$$

$$g^2_{\overline{\rm MS}}(\Lambda) = \frac{g_0^2}{1-\frac{N_c g_0^2}{(4\pi)^2}\ln\left(\frac{\Lambda^2}{\Lambda_0^2}\right)}, \tag{111}$$

$$\lambda_{2\overline{\rm MS}}(\Lambda) = \frac{\lambda_{20}-\frac{N_c g_0^4}{(4\pi)^2}\ln\left(\frac{\Lambda^2}{\Lambda_0^2}\right)}{\left(1-\frac{N_c g_0^2}{(4\pi)^2}\ln\left(\frac{\Lambda^2}{\Lambda_0^2}\right)\right)^2}, \tag{112}$$

$$m^2_{\overline{\rm MS}}(\Lambda) = \frac{m_0^2}{1-\frac{N_c g_0^2}{(4\pi)^2}\ln\left(\frac{\Lambda^2}{\Lambda_0^2}\right)}, \tag{113}$$

$$c_{\overline{\rm MS}}(\Lambda) = \frac{c_0}{1-\frac{N_c g_0^2}{(4\pi)^2}\ln\left(\frac{\Lambda^2}{\Lambda_0^2}\right)}, \tag{114}$$

$$h_{\overline{\rm MS}}(\Lambda) = \frac{h_0}{\sqrt{1-\frac{N_c g_0^2}{(4\pi)^2}\ln\left(\frac{\Lambda^2}{\Lambda_0^2}\right)}}, \tag{115}$$

$$\bar\sigma^2 = f_\pi^2\left[1-\frac{N_c g_0^2}{(4\pi)^2}\ln\left(\frac{\Lambda^2}{\Lambda_0^2}\right)\right], \tag{116}$$

where the parameters λ_{10}, λ_{20}, g_0^2, m_0^2, c_0, and h_0 are the running parameter values at the scale Λ_0. We can choose the Λ_0 to satisfy the following relation:

$$\ln\left(\frac{\Lambda_0^2}{m_q^2}\right) + \mathcal{C}(m_\pi^2) + m_\pi^2\mathcal{C}'(m_\pi^2) = 0. \tag{117}$$

Now, we can calculate the parameters of Eqs. (96)–(102) at the scale $\Lambda = \Lambda_0$ and find λ_{10}, λ_{20}, g_0^2, m_0^2, c_0, and h_0.

C. Effective potential

Using the values of the parameters from Eqs. (110)–(116), the vacuum effective potential in the $\overline{\rm MS}$ scheme can be written as

$$\Omega_{\rm vac} = U(\bar\sigma_{\overline{\rm MS}}) + \Omega^{q,{\rm vac}}_{\overline{\rm MS}} + \delta U(\bar\sigma_{\overline{\rm MS}}), \tag{118}$$

where

$$U(\bar\sigma_{\overline{\rm MS}}) = \frac{m^2_{\overline{\rm MS}}(\Lambda)}{2}\bar\sigma^2_{\overline{\rm MS}} - \frac{c_{\overline{\rm MS}}(\Lambda)}{2}\bar\sigma^2_{\overline{\rm MS}} + \frac{1}{4}\left(\lambda_{1\overline{\rm MS}}(\Lambda) + \frac{\lambda_{2\overline{\rm MS}}(\Lambda)}{2}\right)\bar\sigma^4_{\overline{\rm MS}} - h_{\overline{\rm MS}}(\Lambda)\bar\sigma_{\overline{\rm MS}}, \tag{119}$$

$$\delta U(\bar\sigma_{\overline{\rm MS}}) = \frac{1}{2}(\delta m^2_{\overline{\rm MS}} - \delta c_{\overline{\rm MS}})\bar\sigma^2_{\overline{\rm MS}} + \frac{1}{2}(m^2_{\overline{\rm MS}} - c_{\overline{\rm MS}})\delta\bar\sigma^2_{\overline{\rm MS}} + \frac{1}{4}\left(\delta\lambda_{1\overline{\rm MS}} + \frac{\delta\lambda_{2\overline{\rm MS}}}{2}\right)\bar\sigma^4_{\overline{\rm MS}} + \frac{1}{4}\left(\lambda_{1\overline{\rm MS}} + \frac{\lambda_{2\overline{\rm MS}}}{2}\right)\delta\bar\sigma^4_{\overline{\rm MS}} - \delta h_{\overline{\rm MS}}\bar\sigma_{\overline{\rm MS}} - h_{\overline{\rm MS}}\delta\bar\sigma_{\overline{\rm MS}}. \tag{120}$$

The order $\mathcal{O}(N_c^2)$ terms are dropped as these are two loop terms and we get

$$\delta U(\bar\sigma_{\overline{\rm MS}}) = -\frac{N_c g^4_{\overline{\rm MS}}\bar\sigma^4_{\overline{\rm MS}}}{8(4\pi)^2}\frac{1}{\epsilon} = -\frac{2N_c\Delta^4}{(4\pi)^2}\frac{1}{\epsilon} \tag{121}$$

$$\Omega^{q,{\rm vac}}_{\overline{\rm MS}} = \frac{N_c g^4_{\overline{\rm MS}}\bar\sigma^4_{\overline{\rm MS}}}{8(4\pi)^2}\left[\frac{1}{\epsilon}+\frac{3}{2}+\ln\left(\frac{4\Lambda^2}{g^2_{\overline{\rm MS}}\bar\sigma^2_{\overline{\rm MS}}}\right)\right] = \frac{2N_c\Delta^4}{(4\pi)^2}\left[\frac{1}{\epsilon}+\frac{3}{2}+\ln\left(\frac{\Lambda^2}{\Delta^2}\right)\right]. \tag{122}$$

One can define the scale Λ independent parameter $\Delta = \frac{g_{\overline{\rm MS}}\bar\sigma_{\overline{\rm MS}}}{2}$ using Eqs. (101) and (102). It is instructive to write Eq. (119) in terms of the scale independent Δ as

$$U(\Delta) = 2\frac{m^2_{\overline{\rm MS}}(\Lambda)}{g^2_{\overline{\rm MS}}(\Lambda)}\Delta^2 - 2\frac{c_{\overline{\rm MS}}(\Lambda)}{g^2_{\overline{\rm MS}}(\Lambda)}\Delta^2 + 4\left(\frac{\lambda_{1\overline{\rm MS}}(\Lambda)}{g^4_{\overline{\rm MS}}(\Lambda)} + \frac{\lambda_{2\overline{\rm MS}}(\Lambda)}{2g^4_{\overline{\rm MS}}(\Lambda)}\right)\Delta^4 - 2\frac{h_{\overline{\rm MS}}(\Lambda)}{g_{\overline{\rm MS}}(\Lambda)}\Delta = 2\left(\frac{m_0^2}{g_0^2}-\frac{c_0}{g_0^2}\right)\Delta^2 + 4\left(\frac{\lambda_{10}}{g_0^4}+\frac{\lambda_{20}}{2g_0^4}\right)\Delta^4 - 2\frac{h_0}{g_0}\Delta \tag{123}$$

$$\Omega_{\rm vac}(\Delta) = 2\left(\frac{m_0^2}{g_0^2} - \frac{c_0}{g_0^2}\right)\Delta^2 + 4\left(\frac{\lambda_{10}}{g_0^4} + \frac{\lambda_{20}}{2g_0^4}\right)\Delta^4 - 2\frac{h_0}{g_0}\Delta + \frac{2N_c\Delta^4}{(4\pi)^2}\left[\frac{3}{2} + \ln\left(\frac{\Lambda^2}{\Delta^2}\right)\right]. \tag{124}$$

When the couplings and mass parameter are expressed in terms of the physical meson masses, pion decay constant and Yukawa coupling, one can write

$$\begin{aligned}\Omega_{\rm vac}(\Delta) = {} & \frac{(3m_\pi^2 - m_\sigma^2)f_\pi^2}{4}\left\{1 - \frac{N_c g^2}{(4\pi)^2}(\mathcal{C}(m_\pi^2) + m_\pi^2\mathcal{C}'(m_\pi^2))\right\}\frac{\Delta^2}{m_q^2} + \frac{N_c g^2 f_\pi^2}{2(4\pi)^2}\left\{\frac{3m_\pi^2\mathcal{C}(m_\pi^2) - (m_\sigma^2 - 4m_q^2)\mathcal{C}(m_\sigma^2)}{2} - 2m_q^2\right\}\frac{\Delta^2}{m_q^2} \\ & + \frac{(m_\sigma^2 - m_\pi^2)f_\pi^2}{8}\left\{1 - \frac{N_c g^2}{(4\pi)^2}(\mathcal{C}(m_\pi^2) + m_\pi^2\mathcal{C}'(m_\pi^2))\right\}\frac{\Delta^4}{m_q^4} + \frac{N_c g^2 f_\pi^2}{(4\pi)^2}\left[\frac{(m_\sigma^2 - 4m_q^2)\mathcal{C}(m_\sigma^2) - m_\pi^2\mathcal{C}(m_\pi^2)}{8}\right]\frac{\Delta^4}{m_q^4} \\ & + \frac{2N_c\Delta^4}{(4\pi)^2}\left\{\frac{3}{2} - \ln\left(\frac{\Delta^2}{m_q^2}\right)\right\} - m_\pi^2 f_\pi^2\left\{1 - \frac{N_c g^2}{(4\pi)^2}m_\pi^2\mathcal{C}'(m_\pi^2)\right\}\frac{\Delta}{m_q}.\end{aligned} \tag{125}$$

Here we point out that when we get the final expression of the RQM model vacuum effective potential to one-loop order after renormalization and consistent parameter fixing, the m_η and m_{a_0} dependent correction factors cancel out. We have checked that the expression (125) turns out to be equivalent to the expression of the vacuum effective potential calculated in Ref. [69] [Eq. (7) with $q = 0$] and also given in Eq. (38) of Ref. [71]. It is worthwhile to recall that, due to the dressing of the meson propagator in the RQM model, the pion decay constant and Yukawa coupling both get renormalized in the vacuum. However at the scale Λ_0, Eq. (101) gives $g_{\overline{\rm MS}} = g_{\rm ren} = g$ and Eq. (102) gives $\bar{\sigma}_{\overline{\rm MS}} = f_{\pi,{\rm ren}} = f_\pi$. When the stationarity condition $\frac{\partial\Omega_{\rm vac}(\Delta)}{\partial\Delta}$ is applied to Eq. (124), one gets $h_0 = m_{\pi,c}^2\bar{\sigma}_{\overline{\rm MS}} = m_\pi^2\{1 - \frac{N_c g^2}{(4\pi)^2}m_\pi^2\mathcal{C}'(m_\pi^2)\}f_\pi$. Here, due to the consistent parameter fixing, the pion curvature mass $m_{\pi,c}$ differs from its pole mass m_π as in Ref. [68] and we have $m_{\pi,c}^2 = m_\pi^2\{1 - \frac{N_c g^2}{(4\pi)^2}m_\pi^2\mathcal{C}'(m_\pi^2)\}$. The minimum of the effective potential lies at $\bar{\sigma}_{\overline{\rm MS}} = f_\pi$:

$$\begin{aligned}\Omega_{\rm RQM}(\Delta, T, \mu) = {} & \frac{(3m_\pi^2 - m_\sigma^2)f_\pi^2}{4}\left\{1 - \frac{N_c g^2}{(4\pi)^2}(\mathcal{C}(m_\pi^2) + m_\pi^2\mathcal{C}'(m_\pi^2))\right\}\frac{\Delta^2}{m_q^2} \\ & + \frac{N_c g^2 f_\pi^2}{2(4\pi)^2}\left\{\frac{3m_\pi^2\mathcal{C}(m_\pi^2) - (m_\sigma^2 - 4m_q^2)\mathcal{C}(m_\sigma^2)}{2} - 2m_q^2\right\}\frac{\Delta^2}{m_q^2} \\ & + \frac{(m_\sigma^2 - m_\pi^2)f_\pi^2}{8}\left\{1 - \frac{N_c g^2}{(4\pi)^2}(\mathcal{C}(m_\pi^2) + m_\pi^2\mathcal{C}'(m_\pi^2))\right\}\frac{\Delta^4}{m_q^4} \\ & + \frac{N_c g^2 f_\pi^2}{(4\pi)^2}\left[\frac{(m_\sigma^2 - 4m_q^2)\mathcal{C}(m_\sigma^2) - m_\pi^2\mathcal{C}(m_\pi^2)}{8}\right]\frac{\Delta^4}{m_q^4} + \frac{2N_c\Delta^4}{(4\pi)^2}\left\{\frac{3}{2} - \ln\left(\frac{\Delta^2}{m_q^2}\right)\right\} \\ & - m_\pi^2 f_\pi^2\left\{1 - \frac{N_c g^2}{(4\pi)^2}m_\pi^2\mathcal{C}'(m_\pi^2)\right\}\frac{\Delta}{m_q} - 4N_c T\int\frac{d^3p}{(2\pi)^3}\{\ln[1 + e^{-E_q^+/T)}] + \ln[1 + e^{-E_q^-/T)}]\}.\end{aligned} \tag{126}$$

One gets the chiral condensate or the parameter Δ in the RQM model by searching the global minima of the grand potential in Eq. (126) for a given value of temperature T and chemical potential μ:

$$\frac{\partial\Omega_{\rm RQM}(\Delta, T, \mu)}{\partial\Delta} = 0. \tag{127}$$

In our calculations we have used $m_\pi = 138.0$ MeV, $m_{a_0} = 984.7$ MeV, and $m_\eta = 547.0$ MeV. The Yukawa coupling $g = 6.5$ and pion decay constant $f_\pi = 93.0$ MeV. The constituent quark mass in the vacuum $m_q = \frac{gf_\pi}{2} = 302.25$ MeV.

V. RESULTS AND DISCUSSION

We have plotted the normalized effective potential in the vacuum at $\mu = 0$ and $T = 0$ with respect to the constituent quark mass scale independent parameter Δ in Fig. 6 for the different model scenarios of the parameter fixing and for the different sigma meson masses. The RQM model result is depicted by the solid line in red while the dotted line in blue shows the QM model plot and the dashed green line is

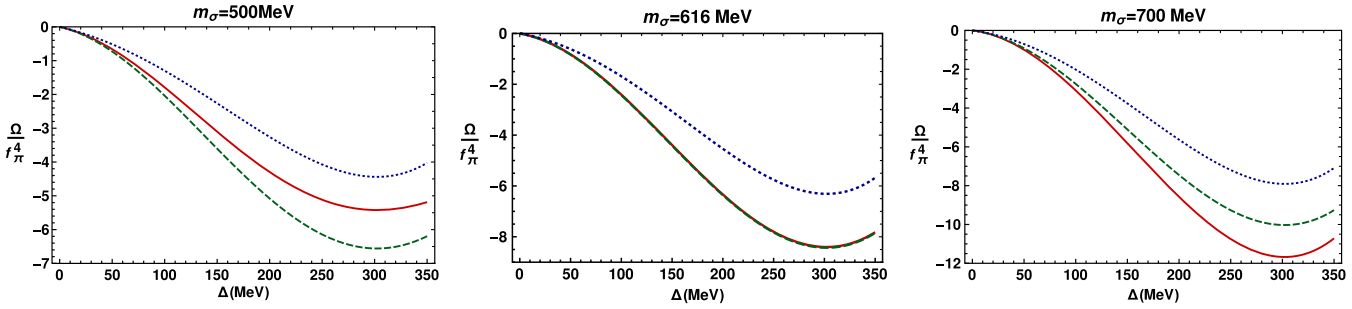

FIG. 6. Blue dotted line, solid red line, and green dashed line, respectively, depict the QM, RQM, and QMVT model result. (a) Effective potential for $m_\sigma = 500$ MeV. (b) Effective potential for $m_\sigma = 616$ MeV. (c) Effective potential for $m_\sigma = 700$ MeV.

plotting the QMVT model result. The effective potential plots corresponding to the $m_\sigma = 500$, 616 and 700 MeV are presented respectively in Figs. 6(a)–6(c). The minimum of the effective potential in all the figures for every model scenario occurs at $\Delta = 302.25 = m_q$ MeV. Its value is highest (i.e., it is most shallow) in the case of no-sea approximation of the QM model for all the m_σ values. It is evident from Fig. 6(a) that for $m_\sigma = 500$ MeV, the effective potential is deepest for the QMVT model while the on-shell parametrization in the RQM model gives a shallower effective potential. Interestingly as we increase the m_σ value, we notice that the RQM model effective potential becomes deeper while the QMVT model effective potential shows an upward trend and finally for the $m_\sigma = 616$ MeV, the effective potential plots for both model scenarios coincide with each other as shown in Fig. 6(b). Increasing the m_σ value beyond 616 MeV, the effective potential plot becomes deepest for the RQM model. The plots of Fig. 6(c) for $m_\sigma = 700$ MeV show that the effective potential becomes deepest for the RQM model and in reversal of the trend seen in Fig. 6(a), the effective potential of the QMVT model is shallower than that of the RQM model.

We have plotted the temperature variation of the quark condensate $\bar{\sigma}$ (which is obtained from the Δ as the Yukawa coupling g remains the same after renormalization) at $\mu = 0$ in Fig. 7 for three values of $m_\sigma = 500$, 616, and 700 MeV. Here also the solid red line, the blue dotted line and the dashed green line, respectively, plot the RQM model, the QM model and the QMVT model results. In general, the chiral transition becomes smoother due to the quark one-loop vacuum correction. For the $m_\sigma = 500$ MeV case in Fig. 7(a), the sharpest QM model quark condensate temperature variation becomes more smooth for the on-shell parametrization of the RQM model while the most smooth variation of the condensate is seen in the QMVT model plot. Sharpest chiral crossover transition occurs early at a pseudocritical temperature of $T_c = 130.2$ MeV in the QM model and a smoother chiral crossover is witnessed for the RQM model at $T_c = 145.6$ MeV while a most delayed and smooth chiral crossover occurs at $T_c = 157.3$ MeV in the QMVT model. For the $m_\sigma = 616$ MeV case in Fig. 7(b), the RQM model result exactly coincides with the QMVT model result for the temperature variation of the quark condensate and the chiral crossover transition occurs at the same temperature of $T_c = 175.6$ MeV. We notice that this behavior follows from the complete coincidence of the vacuum effective potential plot of the RQM model with that of the QMVT model in Fig. 6(b) for the $m_\sigma = 616$ MeV case. For $m_\sigma = 700$ MeV in Fig. 7(c), the most smooth temperature variation of the quark condensate occurs in the RQM model with a very delayed crossover transition at $T_c = 203.6$ MeV while we notice that a less smooth chiral crossover transition occurs earlier at $T_c = 189.8$ MeV in the QMVT model. The

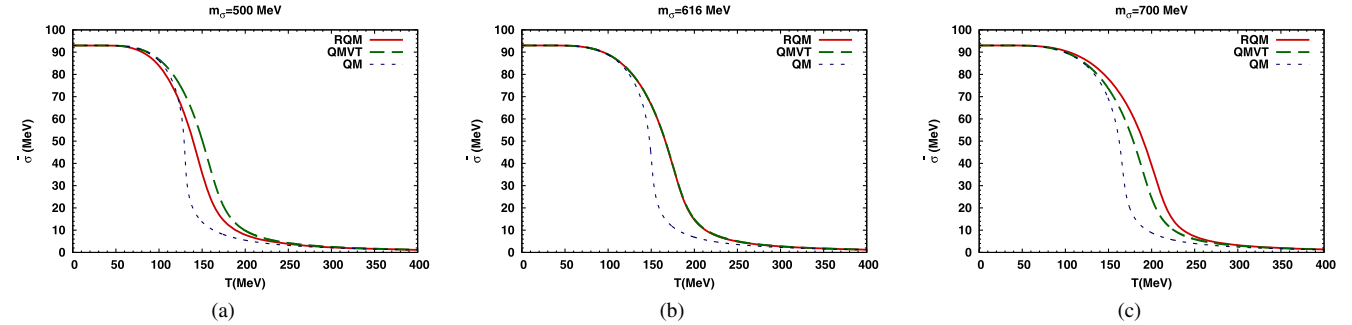

FIG. 7. Blue dotted line, solid red line and green dashed line present the respective temperature variation in the QM, RQM, and QMVT model. (a) Chiral order parameter $m_\sigma = 500$ MeV. (b) Chiral order parameter $m_\sigma = 616$ MeV. (c) Chiral order parameter $m_\sigma = 700$ MeV.

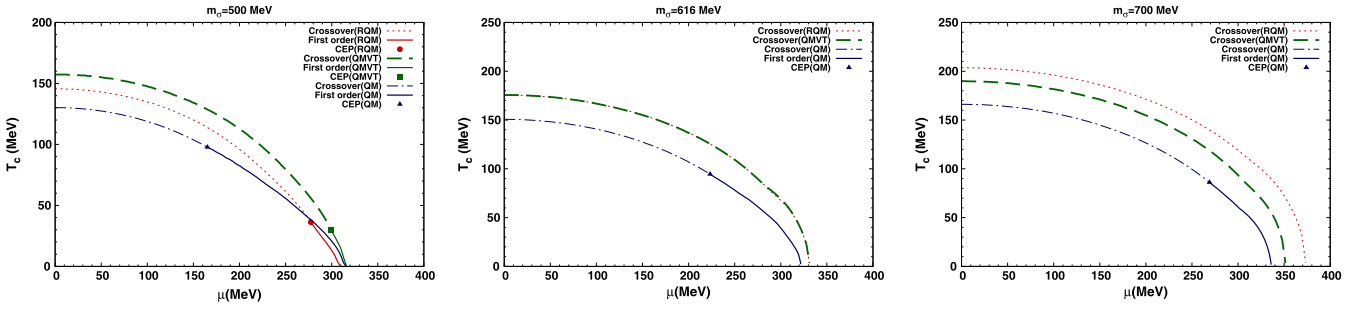

(a) (b) (c)

FIG. 8. Blue dotted line, solid red line, and green dashed line present the respective temperature variation in the QM, RQM, and QMVT model. (a) Phase diagram for the $m_\sigma = 500$ MeV. (b) Phase diagram for the $m_\sigma = 616$ MeV. (c) Phase diagram for the $m_\sigma = 700$ MeV.

Table II presents the summary of the crossover transition temperature T_c at $\mu = 0$ MeV for the $m_\sigma = 400$, 500, 600, 616, and 700 MeV. We point out that when we compare the quark condensate temperature variation of the RQM model with that of the QMVT model, we find that for $m_\sigma =$ 700 MeV the trend becomes opposite of what we observe for the $m_\sigma = 500$ MeV case in Fig. 7(a) where the RQM model condensate variation is less smooth and sharper than the QMVT model condensate variation. Here it is relevant to remind that the vacuum effective potential depth for the RQM model when compared with that of the QMVT model shows the similar role reversal when the $m_\sigma = 500$ MeV plots are contrasted with the $m_\sigma = 700$ MeV plots.

We have drawn the $\mu - T$ plane phase diagram for $m_\sigma =$ 500 MeV in Fig. 8(a) with labeled line types. The QM model critical end point (CEP) location at $\mu = 165.2$ MeV, $T = 97.7$ MeV shifts to a far right position in the $\mu - T$ plane at $\mu = 299.6$ MeV, $T = 29.48$ MeV due to the quark one-loop vacuum correction in the QMVT model setting. Earlier studies [51–53,55,56] reporting similar results have concluded that incorporating the fermionic vacuum fluctuation in the QM model leads to a robust and significant change in the location of CEP. Here we point out that the exact on-shell renormalization of the quark one-loop vacuum fluctuation for the parameter fixing in the RQM model gives a phase diagram in which the CEP location $\mu = 277.3$ MeV, $T = 36.2$ MeV is at a lower chemical potential and higher temperature; i.e., CEP shifts higher up when compared to the position of the CEP in the QMVT model. Furthermore, the RQM model phase diagram for

TABLE II. Critical temperature for $m_\sigma = 400$, 500, 600, 616, and 700 MeV.

m_σ(MeV)	T_c(QM)	T_c(QMVT)	T_c(RQM)
400	113.3	143.6	131.8
500	130.2	157.3	145.6
600	147.8	173.1	169.3
616	150.5	175.6	175.6
700	166.1	189.8	203.6

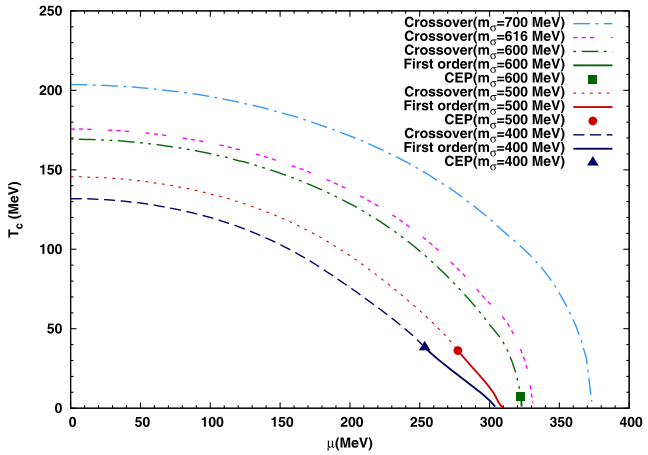

FIG. 9. Phase diagram for the sigma masses of 400, 500, 600, 616, and 700 MeV in the RQM model.

$m_\sigma = 500$ MeV stands in the immediate proximity of the QM model phase diagram.

Here, we emphasize the interesting observation that the RQM model phase diagram, depicting a crossover transition line in the entire $\mu - T$ plane, coincides exactly with the QMVT model phase diagram in Fig. 8(b). This overlap follows from the exact coincidence of the vacuum effective potential plots in Fig. 6(b) for both models RQM and QMVT. The first order line of the QM model plot in Fig. 8(b) is ending in the critical end point (CEP) at $\mu = 223.3$ MeV, $T = 94.45$ MeV. In comparison to the RQM model phase diagram the QMVT model phase diagram in Fig. 8(c) for the $m_\sigma = 700$ MeV stands closer to the QM model phase diagram. It shows the usual trend reversal when compared to the $m_\sigma = 500$ MeV case plots. Again this behavior follows from the trend reversal that we observe in the behavior of the vacuum effective potential in Fig. 6(c). We get a crossover line in the whole $\mu - T$ plane for both of the models, the RQM as well as the QMVT, in Fig. 8(c) while the first order line of the QM model phase diagram is terminating in the critical end point (CEP) at $\mu = 223.3$ MeV, $T = 94.45$ MeV.

In order to see the effect of the sigma meson mass, Fig. 9 plots the five phase diagrams for $m_\sigma = 400$, 500, 600, 616, and 700 MeV in the RQM model. The CEP, $\mu = 253.5$ MeV, $T = 38.2$ MeV for the $m_\sigma = 400$ MeV, moves lower rightwards to $\mu = 277.3$ MeV, $T = 36.2$ MeV for the $m_\sigma = 500$ MeV. When $m_\sigma = 600$ MeV, the CEP shifts to the extreme right bottom of the phase diagram at $\mu = 322.5$ MeV, $T = 7.2$ MeV. The phase transition line becomes a crossover in the entire $\mu - T$ plane for $m_\sigma = 616$ MeV. We have also shown the crossover phase transition line for $m_\sigma = 700$ MeV.

VI. SUMMARY AND CONCLUSION

We have applied the on-shell parameter fixing prescription to the quark-meson (QM) model in which the two flavor of quarks are coupled to the eight mesons of the $SU_L(2) \times SU_R(2)$ linear sigma model. Then the one-loop effective potential is calculated for the renormalized quark-meson (RQM) model whose six running parameters λ_1, λ_2, c, m^2, h, g are determined by relating the $\overline{\text{MS}}$, on-shell schemes and the experimental values of the quark, meson masses and the pion decay constant. After including the one quark-loop vacuum correction in the QM model, the effective potential has been calculated also when the curvature meson masses are used for fixing the model parameters and this model setting has been termed as the quark-meson model with the vacuum term (QMVT). We have computed and compared the effective potentials, the order parameter temperature variations and the phase diagrams for the QM, RQM, and QMVT model settings.

The differences and similarities for the vacuum effective potential plots in the RQM model and the QMVT model depend on the sigma meson mass. When we plot the normalized effective potential with respect to the constituent quark mass parameter Δ, its depth is highest for the QMVT model if $m_\sigma = 500$ MeV and the effective potential is less deep and least in depth respectively for the RQM model and QM model. For $m_\sigma = 616$ MeV, the QMVT model and the RQM model effective potentials become exactly identical to each other. For the higher $m_\sigma = 700$ MeV, the effective potential of the RQM model becomes most deep and the interesting trend reversal is noticed when one contrasts it with the variation of the effective potential for the $m_\sigma = 500$ MeV case. Comparing the $\mu = 0$ temperature variations of the order parameter for the QM, RQM, and QMVT model settings, we find exactly similar differences and similarities depending on the values of the sigma meson mass as observed in the nature of the corresponding normalized effective potential.

It is well reported in the earlier research literature [51–53,55,56] that incorporating the quark one-loop vacuum correction in the QMVT model setting gives rise to a phase diagram in which the CEP shifts towards the right side of the $\mu - T$ plane to quite a higher value of the chemical potential and a lower value of the temperature when one compares it with the location of the CEP in the QM model phase diagram. We have found that when $m_\sigma = 500$ MeV, the shift in the position of the CEP observed in the RQM model is smaller than what is observed in the QMVT model and the RQM model phase boundary stands closer to the QM model phase diagram. Furthermore, driven directly by the nature of the effective potential variation, the phase boundaries depicting the crossover transition lines for both models RQM and QMVT completely overlap with each other when $m_\sigma = 616$ MeV. For the higher $m_\sigma = 700$ MeV, the crossover line of the QMVT model phase diagram comes closer to the QM model phase boundary. This trend is opposite of what we see for the $m_\sigma = 500$ MeV case when the RQM model phase boundary stands closer to the QM model phase diagram. Again the above behavior is caused by the corresponding reversal in the variation of the normalized vacuum effective potential.

ACKNOWLEDGMENTS

Computational support of the computing facility which has been developed by the Nuclear Particle Physics group of the Department of Physics, University of Allahabad (UOA), under the Center of Advanced Studies (CAS) funding of University Grants Commission (UGC), India, is acknowledged. The Department of Science and Technology, Government of India, DST-PURSE Program Phase 2/43(C), financial support to the science faculty of the UOA is also acknowledged. We would also like to acknowledge the support of Professor Prashant Shukla, Department of Mechanical Engineering IIT BHU, for reading the manuscript carefully and correcting the use of incorrect commas.

APPENDIX A: THE QMVT PARAMETER FIXING

The tree-level expression of the curvature masses of mesons for the QM model are given by the mass matrix evaluated in Ref. [17]. In this work, the above mass matrix is renamed as $(m^m_{\alpha,ab})^2$ where superscript m stands for the contribution of the pure mesonic potential. In the QMVT model, the meson curvature masses get modified by the quark one-loop vacuum contribution. The total expression of the meson curvature masses in the QMVT model is written as

$$m^2_{\alpha,ab} = (m^m_{\alpha,ab})^2 + (\delta m^v_{\alpha,ab})^2, \tag{A1}$$

where $\alpha = s$, p; "s" stands for the scalar and "p" stands for the pseudoscalar mesons and a, $b = 0$, 1, 2, 3. $m^2_{s,00} \equiv m^2_\sigma$; $m^2_{s,11} = m^2_{s,22} = m^2_{s,33} \equiv m^2_{a_0}$ and $m^2_{p,00} \equiv m^2_\eta$; $m^2_{p,11} = m^2_{p,22} = m^2_{p,33} \equiv m^2_\pi$. The $(m^m_{\alpha,ab})^2$ and $(\delta m^v_{\alpha,ab})^2$ are defined in the similar fashion. The expression of the curvature masses $(m^m_{\alpha,ab})^2$ has been given in Table III. Superscript "v" stands for the quark/antiquark vacuum contribution to the curvature masses. It is written as

TABLE III. Expressions of the curvature masses $(m^m_{\alpha,ab})^2$ are calculated from the second derivative of the pure mesonic potential as has been evaluated in Ref. [17].

$(m^m_{\alpha,ab})^2$		Meson mass found from the pure mesonic potential
$(m^m_{s,00})^2$	$(m^m_\sigma)^2$	$m^2 - c + 3(\lambda_1 + \frac{\lambda_2}{2})\bar{\sigma}^2$
$(m^m_{s,11})^2$	$(m^m_{a_0})^2$	$m^2 + c + (\lambda_1 + \frac{3\lambda_2}{2})\bar{\sigma}^2$
$(m^m_{p,00})^2$	$(m^m_\eta)^2$	$m^2 + c + (\lambda_1 + \frac{\lambda_2}{2})\bar{\sigma}^2$
$(m^m_{p,11})^2$	$(m^m_\pi)^2$	$m^2 - c + (\lambda_1 + \frac{\lambda_2}{2})\bar{\sigma}^2$

$$(\delta m^v_{\alpha,ab})^2 = \left.\frac{\partial^2 \Omega^{\rm vac}_{q\bar{q}}}{\partial\xi_{\alpha,a}\partial\xi_{\alpha,b}}\right|_{\rm min},$$
$$= \sum_{q=u,d}\frac{2N_c}{(4\pi)^2}\left[\{m^2_{q,\alpha a}m^2_{q,\alpha b} + m^2_q m^2_{q,\alpha ab}\}\times\left\{1+\ln\left(\frac{\Lambda^2}{m_q^2}\right)\right\} - m^2_{q,\alpha a}m^2_{q,\alpha b}\right], \quad \text{(A2)}$$

where $m^2_{q,\alpha a} = \frac{\partial m^2_q}{\partial\xi_{\alpha,a}}$ and $m^2_{q,\alpha ab} = \frac{\partial m^2_{q,\alpha a}}{\partial\xi_{\alpha,b}}$. When one computes the second derivative of Eq. (30) for the quark contribution, the full dependence of all the scalar and pseudoscalar meson fields, cf. Eq. (4), in the quark masses has to be considered. The resulting quark mass matrix is diagonalized similar to the three flavor case given in Ref. [42]. In all the quark mass derivatives with respect to the meson fields, the meson fields are replaced by the nonvanishing vacuum expectation value $\bar{\sigma}$ and the final values are collected in Table IV.

Using Table IV in Eq. (A2) we get vacuum contributions of meson masses as

$$(\delta m^v_\sigma)^2 \equiv (\delta m^v_{s,00})^2 = \frac{N_c g^4\bar{\sigma}^2}{2(4\pi)^2}\left[1+3\ln\left(\frac{\Lambda^2}{m_q^2}\right)\right], \quad \text{(A3)}$$

$$(\delta m^v_{a_0})^2 \equiv (\delta m^v_{s,11})^2 = \frac{N_c g^4\bar{\sigma}^2}{2(4\pi)^2}\left[1+3\ln\left(\frac{\Lambda^2}{m_q^2}\right)\right], \quad \text{(A4)}$$

$$(\delta m^v_\eta)^2 \equiv (\delta m^v_{p,00})^2 = \frac{N_c g^4\bar{\sigma}^2}{2(4\pi)^2}\left[1+\ln\left(\frac{\Lambda^2}{m_q^2}\right)\right], \quad \text{(A5)}$$

TABLE IV. Squared quark mass derivatives with respect to the meson fields evaluated at the minimum. The last two columns present the first and second derivative of the squared quark mass summed over two quark flavor.

s/p	a	b	$m^2_{q,\alpha a}m^2_{q,ab}/g^4$	$m^2_{q,\alpha ab}/g^2$
s	0	0	$\frac{1}{2}\bar{\sigma}^2$	1
s	1	1	$\frac{1}{2}\bar{\sigma}^2$	1
p	0	0	0	1
p	1	1	0	1

$$(\delta m^v_\pi)^2 \equiv (\delta m^v_{p,11})^2 = \frac{N_c g^4\bar{\sigma}^2}{2(4\pi)^2}\left[1+\ln\left(\frac{\Lambda^2}{m_q^2}\right)\right]. \quad \text{(A6)}$$

We get $(m^m_\sigma)^2$, $(m^m_\eta)^2$, $(m^m_{a_0})^2$, and $(m^m_\eta)^2$ after substitution of Eqs. (A3)–(A6) into Eq. (A1) as

$$(m^m_\sigma)^2 = m^2_\sigma - \frac{N_c g^4\bar{\sigma}^2}{2(4\pi)^2}\left[1+3\ln\left(\frac{\Lambda^2}{m_q^2}\right)\right], \quad \text{(A7)}$$

$$(m^m_{a_0})^2 = m^2_{a_0} - \frac{N_c g^4\bar{\sigma}^2}{2(4\pi)^2}\left[1+3\ln\left(\frac{\Lambda^2}{m_q^2}\right)\right], \quad \text{(A8)}$$

$$(m^m_\eta)^2 = m^2_\eta - \frac{N_c g^4\bar{\sigma}^2}{2(4\pi)^2}\left[1+\ln\left(\frac{\Lambda^2}{m_q^2}\right)\right], \quad \text{(A9)}$$

$$(m^m_\pi)^2 = m^2_\pi - \frac{N_c g^4\bar{\sigma}^2}{2(4\pi)^2}\left[1+\ln\left(\frac{\Lambda^2}{m_q^2}\right)\right]. \quad \text{(A10)}$$

The parameters in vacuum are obtained as

$$\lambda_1 = \frac{(m^m_\sigma)^2 + (m^m_\eta)^2 - (m^m_{a_0})^2 - (m^m_\pi)^2}{2f^2_\pi} \quad \text{(A11)}$$

$$\lambda_2 = \frac{(m^m_{a_0})^2 - (m^m_\eta)^2}{f^2_\pi} \quad \text{(A12)}$$

$$m^2 = (m^m_\pi)^2 + \frac{(m^m_\eta)^2 - (m^m_\sigma)^2}{2} \quad \text{(A13)}$$

$$c = \frac{(m^m_\eta)^2 - (m^m_\pi)^2}{2}. \quad \text{(A14)}$$

We get the parameters of the QMVT on substitution of Eqs. (A7)–(A10) into Eqs. (A11)–(A14) and found that λ_1, c of the QMVT are the same with respect to λ_1, c of the QM. We observe change in λ_2 and m^2 as

$$\lambda_2 = \lambda_{2s} - \frac{N_c g^4}{(4\pi)^2}\ln\left(\frac{4\Lambda^2}{g^2 f^2_\pi}\right) \quad \text{(A15)}$$

$$m^2 = m^2_s - \frac{N_c g^4 f^2_\pi}{2(4\pi)^2}, \quad \text{(A16)}$$

where λ_{2s} and m^2_s are the same old λ_2 and m^2 parameters of the QM model. Putting the value of the new parameters λ_2 and m^2 in Eq. (A10) one can write the expression of pion mass independent of renormalization scale as

$$m^2_\pi = m^2_s - \frac{N_c g^4}{2(4\pi)^2}(f^2_\pi - \bar{\sigma}^2) - c + \left(\lambda_1 + \frac{\lambda_{2s}}{2}\right)\bar{\sigma}^2 + \frac{N_c g^4}{2(4\pi)^2}\log\left(\frac{f^2_\pi}{\bar{\sigma}^2}\right)\bar{\sigma}^2. \quad \text{(A17)}$$

APPENDIX B: INTEGRALS AND SUM INTEGRALS

The divergent loop integrals are regularized by incorporating the dimensional regularization,

$$\int_p = \left(\frac{e^{\gamma_E}\Lambda^2}{4\pi}\right)^{\epsilon} \int \frac{d^d p}{(2\pi)^d}, \tag{B1}$$

where $d = 4 - 2\epsilon$, γ_E is the Euler-Mascheroni constant, and Λ is renormalization scale associated with the $\overline{\text{MS}}$:

$$\mathcal{A}(m_q^2) = \int_p \frac{1}{p^2 - m_q^2} = \frac{i m_q^2}{(4\pi)^2}\left[\frac{1}{\epsilon} + 1 + \ln(4\pi e^{-\gamma_E}) + \ln\left(\frac{\Lambda^2}{m_q^2}\right)\right].$$

We rewrite this after redefining $\Lambda^2 \to \Lambda^2 \frac{e^{\gamma_E}}{4\pi}$:

$$\mathcal{A}(m_q^2) = \frac{i m_q^2}{(4\pi)^2}\left[\frac{1}{\epsilon} + 1 + \ln\left(\frac{\Lambda^2}{m_q^2}\right)\right] \tag{B2}$$

$$\mathcal{B}(p^2) = \int_k \frac{1}{(k^2 - m_q^2)[(k+p)^2 - m_q^2)]} = \frac{i}{(4\pi)^2}\left[\frac{1}{\epsilon} + \ln\left(\frac{\Lambda^2}{m_q^2}\right) + C(p^2)\right] \tag{B3}$$

$$\mathcal{B}'(p^2) = \frac{i}{(4\pi)^2} C'(p^2) \tag{B4}$$

$$C(p^2) = \begin{cases} 2 - 2\sqrt{\frac{4m_q^2}{p^2} - 1}\arctan\left(\frac{1}{\sqrt{\frac{4m_q^2}{p^2}-1}}\right), & (p^2 < 4m_q^2) \\ 2 + \sqrt{1 - \frac{4m_q^2}{p^2}}\ln\left(\frac{1-\sqrt{1-\frac{4m_q^2}{p^2}}}{1+\sqrt{1-\frac{4m_q^2}{p^2}}}\right), & (p^2 > 4m_q^2) \end{cases} \tag{B5}$$

$$C'(p^2) = \begin{cases} \frac{4m_q^2}{p^4\sqrt{\frac{4m_q^2}{p^2}-1}}\arctan\left(\frac{1}{\sqrt{\frac{4m_q^2}{p^2}-1}}\right) - \frac{1}{p^2}, & (p^2 < 4m_q^2) \\ \frac{2m_q^2}{p^4\sqrt{1-\frac{4m_q^2}{p^2}}}\ln\left(\frac{1-\sqrt{1-\frac{4m_q^2}{p^2}}}{1+\sqrt{1-\frac{4m_q^2}{p^2}}}\right) - \frac{1}{p^2}, & (p^2 > 4m_q^2). \end{cases} \tag{B6}$$

[1] N. Cabibbo and G. Parisi, Phys. Lett. **59B**, 67 (1975).
[2] L. D. McLerran and B. Svetitsky, Phys. Rev. D **24**, 450 (1981); B. Svetitsky, Phys. Rep. **132**, 1 (1986).
[3] B. Muller, Rep. Prog. Phys. **58**, 611 (1995).
[4] H. Meyer-Ortmanns, Rev. Mod. Phys. **68**, 473 (1996).
[5] D. H. Rischke, Prog. Part. Nucl. Phys. **52**, 197 (2004).
[6] A. Ali Khan, A. Aoki, R. Burkhalter, S. Ejiri, M. Fukugita, S. Hashimoto *et al.*, Phys. Rev. D **64**, 074510 (2001).
[7] S. Digal, E. Laermann, and H. Satz, Eur. Phys. J. C **18**, 583 (2001).
[8] F. Karsch, Lect. Notes Phys. **583**, 209 (2002).
[9] Z. Fodor, S. D. Katz, and K. K. Szabo, Phys. Lett. B **568**, 73 (2003).
[10] C. R. Allton, M. Doring, S. Ejiri, S. J. Hands, O. Kaczmarek, F. Karsch, E. Laermann, and K. Redlich, Phys. Rev. D **71**, 054508 (2005).
[11] F. Karsch, J. Phys. G **31**, S633 (2005).

[12] Y. Aoki, Z. Fodor, S. D. Katz, and K. K. Szabo, Phys. Lett. B **643**, 46 (2006).
[13] M. Cheng, N. H. Christ, S. Datta, J. van der Heide, C. Jung, F. Karsch *et al.*, Phys. Rev. D **74**, 054507 (2006).
[14] M. Cheng, N. H. Christ, S. Datta, J. van der Heide, C. Jung, F. Karsch *et al.*, Phys. Rev. D **77**, 014511 (2008).
[15] M. G. Alford, A. Schmitt, K. Rajagopal, and T. Schafer, Rev. Mod. Phys. **80**, 1455 (2008).
[16] K. Fukushima and T. Hatsuda, Rep. Prog. Phys. **74**, 014001 (2011).
[17] D. Roder, J. Ruppert, and D. H. Rischke, Phys. Rev. D **68**, 016003 (2003).
[18] K. Fukushima, K. Kamikado, and B. Klein, Phys. Rev. D **83**, 116005 (2011).
[19] M. Grahl and D. H. Rischke, Phys. Rev. D **88**, 056014 (2013).
[20] A. M. Polyakov, Phys. Lett. **72B**, 477 (1978).
[21] K. Fukushima, Phys. Lett. B **591**, 277 (2004).
[22] B. Svetitsky and L. G. Yaffe, Nucl. Phys. **B210**, 423 (1982).
[23] R. D. Pisarski, Phys. Rev. D **62**, 111501(R) (2000).
[24] B. Layek, A. P. Mishra, A. M. Srivastava, and V. K. Tiwari, Phys. Rev. D **73**, 103514 (2006).
[25] C. Ratti, M. A. Thaler, and W. Weise, Phys. Rev. D **73**, 014019 (2006).
[26] K. Fukushima, Phys. Rev. D **78**, 114019 (2008).
[27] O. Scavenius, A. Mocsy, I. N. Mishustin, and D. H. Rischke, Phys. Rev. C **64**, 045202 (2001).
[28] J. T. Lenaghan, D. H. Rischke, and J. Schaffner-Bielich, Phys. Rev. D **62**, 085008 (2000); J. T. Lenaghan and D. H. Rischke, J. Phys. G **26**, 431 (2000).
[29] A. Jakovac, A. Patkos, Z. Szep, and P. Szepfalusy, Phys. Lett. B **582**, 179 (2004).
[30] T. Herpay, A. Patkós, Zs. Szép, and P. Szépfalusy, Phys. Rev. D **71**, 125017 (2005).
[31] T. Herpay and Zs. Szép, Phys. Rev. D **74**, 025008 (2006).
[32] P. Kovács and Zs. Szép, Phys. Rev. D **75**, 025015 (2007).
[33] T. Kahara and K. Tuominen, Phys. Rev. D **78**, 034015 (2008); **80**, 114022 (2009); **82**, 114026 (2010).
[34] E. S. Bowman and J. I. Kapusta, Phys. Rev. C **79**, 015202 (2009); J. I. Kapusta and E. S. Bowman, Nucl. Phys. **A830**, 721C (2009).
[35] G. Fejos and A. Patkos, Phys. Rev. D **82**, 045011 (2010).
[36] A. Jakovac and Zs. Szep, Phys. Rev. D **82**, 125038 (2010).
[37] L. Ferroni, V. Koch, and M. B. Pinto, Phys. Rev. C **82**, 055205 (2010).
[38] G. Marko and Zs. Szep, Phys. Rev. D **82**, 065021 (2010).
[39] A. Mocsy, I. N. Mishustin, and P. J. Ellis, Phys. Rev. C **70**, 015204 (2004).
[40] B.-J. Schaefer and J. Wambach, Nucl. Phys. **A757**, 479 (2005).
[41] B.-J. Schaefer and J. Wambach, Phys. Rev. D **75**, 085015 (2007).
[42] B. J. Schaefer and M. Wagner, Phys. Rev. D **79**, 014018 (2009).
[43] B. J. Schaefer, J. M. Pawlowski, and J. Wambach, Phys. Rev. D **76**, 074023 (2007).
[44] B. J. Schaefer, M. Wagner, and J. Wambach, Phys. Rev. D **81**, 074013 (2010).
[45] H. Mao, J. Jin, and M. Huang, J. Phys. G **37**, 035001 (2010).
[46] U. S. Gupta and V. K. Tiwari, Phys. Rev. D **81**, 054019 (2010).
[47] R. D. Pisarski and F. Wilczek, Phys. Rev. D **29**, 338 (1984).
[48] M. A. Halasz, A. D. Jackson, R. E. Shrock, M. A. Stephanov, and J. J. M. Verbaarschot, Phys. Rev. D **58**, 096007 (1998).
[49] V. Skokov, B. Friman, E. Nakano, K. Redlich, and B.-J. Schaefer, Phys. Rev. D **82**, 034029 (2010).
[50] R. Khan and L. T. Kyllingstad, AIP Conf. Proc. **1343**, 504 (2011).
[51] U. S. Gupta and V. K. Tiwari, Phys. Rev. D **85**, 014010 (2012).
[52] B.-J. Schaefer and M. Wagner, Phys. Rev. D **85**, 034027 (2012).
[53] S. Chatterjee and K. A. Mohan, Phys. Rev. D **85**, 074018 (2012).
[54] J. O. Andersen and A. Tranberg, J. High Energy Phys. 08 (2012) 002.
[55] V. K. Tiwari, Phys. Rev. D **86**, 094032 (2012).
[56] S. Chatterjee and K. A. Mohan, Phys. Rev. D **86**, 114021 (2012).
[57] V. K. Tiwari, Phys. Rev. D **88**, 074017 (2013).
[58] T. K. Herbst, J. M. Pawlowski, and B.-J. Schaefer, Phys. Rev. D **88**, 014007 (2013).
[59] J. Weyrich, N. Strodthoff, and L. von Smekal, Phys. Rev. C **92**, 015214 (2015).
[60] P. Kovacs, Zs Szep, and Gy Wolf, Phys. Rev. D **93**, 114014 (2016).
[61] Andreas Zacchi and Jürgen Schaffner-Bielich, Phys. Rev. D **97**, 074011 (2018).
[62] Andreas Zacchi and Jürgen Schaffner-Bielich, Phys. Rev. D **100**, 123024 (2019).
[63] S. K. Rai and V. K. Tiwari, Eur. Phys. J. Plus **135**, 844 (2020).
[64] K. Kajantie, M. Laine, K. Rummukainen, and M. E. Shaposhnikov, Nucl. Phys. **B458**, 90 (1996).
[65] P. Adhikari, J. O. Andersen, and P. Kneschke, Phys. Rev. D **95**, 036017 (2017).
[66] S. Carignano, M. Buballa, and B.-J. Schaefer, Phys. Rev. D **90**, 014033 (2014).
[67] J. O. Andersen, W. R. Naylor, and A. Tranberg, Rev. Mod. Phys. **88**, 025001 (2016).
[68] S. Carignano, M. Buballa, and W. Elkamhawy, Phys. Rev. D **94**, 034023 (2016).
[69] P. Adhikari, J. O. Andersen, and P. Kneschke, Phys. Rev. D **96**, 016013 (2017).
[70] P. Adhikari, J. O. Andersen, and P. Kneschke, Phys. Rev. D **98**, 074016 (2018).
[71] A. Folkestad and J. O. Andersen, Phys. Rev. D **99**, 054006 (2019).
[72] R. Kobes, G. Kunstatter, and A. Rebhan, Phys. Rev. Lett. **64**, 2992 (1990); Nucl. Phys. **B355**, 1 (1991).
[73] A. K. Rebhan, Phys. Rev. D **48**, R3967 (1993).